2017

Fingerprinting Wolframite: An Atomic/crystallographic, Chemical And Spectroscopic Study Along The Solid Solution Series

Gina Marie Accorsi
University of Vermont

FINGERPRINTING WOLFRAMITE: AN ATOMIC/CRYSTALLOGRAPHIC, CHEMICAL AND SPECTROSCOPIC STUDY ALONG THE SOLID SOLUTION SERIES

A Thesis Presented

by

Gina Accorsi

to

The Faculty of the Graduate College

of

The University of Vermont

In Partial Fulfillment of the Requirements
for the Degree of Master of Science
Specializing in Geology

May, 2017

Defense Date: March 20, 2017
Thesis Examination Committee:

John M. Hughes, Ph.D., Advisor
Robert V. Bartlett, Ph.D., Chairperson
Laura E. Webb, Ph.D.
Cynthia J. Forehand, Ph.D., Dean of the Graduate College

ABSTRACT

In accordance with the 2010 Dodd-Frank Act, conflict minerals refer to gold, tantalum, tin, and tungsten bearing minerals sourced from the Democratic Republic of Congo (DRC) that have been mined illegally and used to funnel funds to rebel forces. In response to an increasing demand for these metals used in cellphones, computers, and other popular technologies, Dodd-Frank mandates that industrial consumers demonstrate due diligence and assure that the materials they use have been extracted legally. Because current chain-of-custody methods have not been effective in sourcing ores, a study was undertaken whereby the range of mineralogical characteristics of 15 samples along the wolframite solid solution series were determined in order to ascertain if differences in these characteristics would permit fingerprinting of the source deposit of wolframite, of which the DRC is the world's fifth largest producer.

For these 15 samples, single-crystal X-ray structure and powder X-ray diffraction studies have been conducted; major, minor and trace element chemistry has been determined using ICP-MS and ICP-OES; and Raman spectroscopy has been carried out. Finally, statistical methods were used to determine relationships between samples, and the results of that mathematical work show that there is no firm method at the present time of determining the provenance of a sample based on the information of the crystal structure, diffraction patterns, vibrational frequencies/scattering, or major and trace elemental chemistry.

This study elucidates the range of mineralogical properties along the hübnerite-ferberite solid solution series while working towards to development of an analytical technique that is affordable, practical, accessible and effective for industrial consumers seeking product certification and compliance with the 2010 Dodd-Frank Act.

TABLE OF CONTENTS

Page

LIST OF TABLES

LIST OF FIGURES

CHAPTER 1: INTRODUCTION

In 2010, U.S. President Barack Obama signed the Dodd-Frank Wall Street Reform and Consumer Protection Act (hereafter Dodd-Frank) into Federal Law. The law is defined as "an Act to promote the financial stability of the United States by improving accountability and transparency in the financial system in order to protect consumers from abusive financial service practices…" (US Securities and Exchange Commission 2009).

Title XV, Section 1502 (and to some extent, Sections 1503 and 1504) of Dodd-Frank pertains specifically to the use of conflict minerals from the Democratic Republic of Congo or any adjoining country. Conflict minerals refer specifically to cassiterite, wolframite, gold, and tantalum-bearing "coltan" minerals according to the USGS (Little 2010). Dodd-Frank requires that companies that use cassiterite, wolframite, gold or "coltan" in their products report measures that they are taking to exercise due diligence on the source and chain of custody of any of the minerals in question. An independent private sector company must also audit the report. Though compliance with these rules was not required until the first full fiscal year after which this law was passed, that first year has come and gone, and no companies have been able to completely comply due more to a lack of ability than effort (Kester & Murphy 2014; (Gianopoulos 2015).

One method for clarifying the provenance of a mineral is to have a certified person from an independent private sector company physically travel with the mineral shipment from its place of origin to the smelting/refining destination, in order to verify supply chain details and provide transparency through chain-of-custody. This method is

not affordable, practical, or even possible in many situations. Current certification schemes are also murky and unclear for minerals other than diamonds. In 2014, several companies informed the SEC that such "chain-of-custody" assurances are not practical for Dodd-Frank compliance (Willhite 2014). "Five years later I'm concerned this well-intended conflict minerals rule is actually harming the very people it was intended to help," said U.S. Congressman Rep. Bill Huizenga in 2015. "A preemptive ban on buying Congolese minerals has been the easiest response: many companies gave preference to shifting their supply chains elsewhere rather than trying to be in accordance with this new regulatory framework" (Cuvelier 2014).

Because most companies don't have the means to comply, many have stopped doing business with the DRC in an attempt to avoid the issue altogether, making matters worse for prisoners of illegal mining operations as warlords become desperate and agitated, harming legal, artisanal mining operations, and stunting regional economic progress overall (Autesserre 2012). Even with a growing number of private auditing companies and conflict mineral legal specialists appearing, Dodd Frank scrutiny and subsequent reform is currently underway due to insufficient social mechanisms for mineral supply chain management (Chasan 2015).

Other notable efforts to trace conflict minerals in supply chains outside of the US, as outlined by Burt (2016), include OECD Due Diligence Guidance for Responsible Supply Chains of Minerals from Conflict-Affected and High Risk Areas (OECD 2011), Other examples include the International Conference of the Great Lakes Region (ICGLR) Regional Certification Mechanism (Lezhnev 2015), and in 2009 the tin industry's '3Ts' (Tin, Tantalum, Tungsten) due diligence program known as the ITRI Tin

Supply Chain Initiative (iTSCi), which is a 'bag and tag' program whereby independent auditing as well as safety reporting is conducted at the local and regional level. This method has proven to be extremely expensive, with miners paying any necessary fees rather than the buyer (ITRI 2015). Another issue with the program is the excessive amount of data generated in the process that are only available on paper, rather than digitally, which has slowed the efficacy of the system and reporting. The Electronic Industry Citizenship Coalition and Global e-Sustainability Initiative (EICC/GeSI) put forth the Conflict Free Smelter Initiative' (CFSI) requiring smelters/chemical processing companies and industries to document and share their conflict-free sourcing efforts in (Electronic Industry Citizenship Coalition 2011).

Another proposed method for tracing minerals is to analytically fingerprint the ore minerals using chemical, structural and spectroscopic data in order to identify provenance, based on unique characteristics found within each sample of interest. This method has not yet been employed by companies attempting to comply with Dodd Frank; indeed, for some of the compounds in question, the background data showing a base range in crystallographic and chemical variation found within the mineral groups are not yet available and still need to be established.

Laser-Induced Breakdown Spectroscopy (LIBS) was used by Richard R. Harker, a chemistry professor at Juniata College in 2010, to distinguishing columbite-tantalite (coltan) ores from different localities (Harker 2012). In 2008 the German Federal Ministry for Economic Cooperation and Development (BMZ) also began to develop a fingerprinting method for tantalum using LIBS (Melcher et al. 2008). These analyses

have not been tested on other conflict minerals, such as wolframite, also singled out within the Dodd-Frank Act.

Wolframite is the term used to describe the solid solution series between ferberite ($FeWO_4$) and hübnerite ($MnWO_4$). Tungsten derived from wolframite is used in cemented carbides, wires, electrodes, filaments, contacts used in lighting, electronics, electrical, heating, and welding applications, alloy parts and coatings, super alloys for turbine blades, catalysts, inorganic pigments, and high-temperature lubricants (Shedd 2000). Tungsten also has the highest melting point of all metals, very high tensile strength and corrosion resistance, and has a thermal expansion very similar to that of borosilicates, making it useful for glass to metal seals (Gbaruko & Igwe 2007).

In order to elucidate the range in crystallographic and chemical variation found within the wolframite solid solution series and evaluate the efficacy of the development of a method for analytically fingerprinting minerals along the wolframite solid solution series, this project examines the crystal structure, chemistry, powder diffraction and Raman spectroscopy of a suite of ferberites and hübnerites in the most comprehensive study of the wolframite solid solution series undertaken to date. Samples for this study include 15 members along the wolframite solid solution series from around world, 13 of which were procured from the Harvard Mineralogical and Geological Museum (HMGM) (Table 1).

Table 1. Sample Descriptions

Harvard Reference #	Place of Origin	Composition	Abbreviation
NA*	Tae Hwa Mine, Chung Cheung Buck Oo Korea	$(Fe_{0.35}Mn_{0.65})WO_4$ hübnerite	KOR
NA*	Mundo Nuevo Mine, Huamachuco, Sanchez Carrion Province, La Libertad Department Peru	$(Fe_{0.09}Mn_{0.91})WO_4$ hübnerite	PER
88878	Zinnwald Saxony	$(Fe_{0.35}Mn_{0.58})WO_4$ hübnerite	SAX
89697	Arizona USA	$(Fe_{0.05}Mn_{0.95})WO_4$ hübnerite	USA1
90695	Torrington Mine, New South Whales (Clive Co.) Australia	$(Fe_{0.86}Mn_{0.16})WO_4$ ferberite	AUS1
91734	Borralha Portugal	$(Fe_{0.75}Mn_{0.35})WO_4$ ferberite	POR
94759	Bolivia	$(Fe_{0.89}Mn_{0.09})WO_4$ ferberite	BOL
94809	Northern Queensland Australia	$(Fe_{0.65}Mn_{0.35})WO_4$ ferberite	AUS2
97280	Williams Mine, Big Sandy Arizona USA	$(Fe_{0.12}Mn_{0.96})WO_4$ hübnerite	USA2
97281	Germania Mine, Stevens County, Washington USA	$(Fe_{0.81}Mn_{0.19})WO_4$ ferberite	USA3
104536	Kirwa Wolfram Mine, Kabale Uganda	$(Fe_{1.00})WO_4$ ferberite	UGA
111400	Cornwall England	$(Fe_{0.64}Mn_{0.37})WO_4$ ferberite	ENG
115464	Schlaggenwald Bohemia	$(Fe_{0.81}Mn_{0.15})WO_4$ ferberite	BOH
120376	U.S. Tin Corp., Lost River Alaska	$(Fe_{0.23}Mn_{0.77})WO_4$ hübnerite	USA4
133545	(Zinnwald) Cinvald Zapadocesky, Czech Republic	$(Fe_{0.37}Mn_{0.64})WO_4$ hübnerite	CR

***Purchased for study, no reference # available**

CHAPTER 2: METHODS

2.1. Background

In 2011, Harmon et al. worked with Applied Spectra to use laser-induced breakdown spectroscopy (LIBS) to give tantalum-bearing minerals from the DRC their own geochemical fingerprint. LIBS generates those fingerprints with a laser-induced plasma that breaks down a sample into constituent atoms and excites those atoms to emit light at specific wavelengths. Pattern recognition and statistical methods, typically partial least squares discriminant analysis, can elucidate subtle differences between samples.

Carrying out similar studies in 2008, Melcher et al. incorporated scanning electron microscopy and laser ablation inductively coupled plasma mass spectrometry (LA-ICP-MS) on cassiterite samples. Melcher questions LIBS' detection limits of trace elements, especially the rare earths' complex spectra, as well as accuracy. Melcher et al. 2008 is not convinced that the current LIBS technique provides a suitable fingerprint, somewhat due to that fact that scanning electron microscopy may be too expensive to be practical or realistically applied.

LIBS has also been used to determine the provenance of diamonds (Mcmanis 2015) though the issue with applying this technique to the sociopolitical problem of conflict minerals is the large number of samples from many locations that are required. This is will be discussed in more detail later in this paper.

These considerations relate to where along the supply chain materials of interest are being fingerprinted. After smelting, during which ores from different mines are often mixed together as some aggregate, identifying specific source locations becomes

impossible – there is no longer any way to determine provenance. It is unknown how much of the mineral's fingerprint is still going to be left, if any, after smelting.

This means that any fingerprinting of minerals will most likely have to happen on the ground, in the field, somewhere between leaving the source and being smelted, before having its fingerprints altered. Devising a method that is affordable and accessible is paramount in the efficacy of developing this new technique, which is something to keep in mind when being realistic about how feasible, practical adoptable an analytical approach actually is.

Another goal of this study was to gather as much data as possible on the crystal chemistry of the compositions along the wolframite solid solution series. Inductively coupled plasma mass spectrometry analysis or single crystal diffraction may not be the most affordable or accessible way to fingerprint minerals, which is a goal of this study. However, if data from single crystal diffraction or inductively coupled plasma mass spectrometry support what we find from powder X-ray diffraction, which is much more portable, affordable to use, and simpler to operate, then we have at least narrowed down what will work, what won't, and how practically we are able to obtain the data necessary for regional distinction.

To undertake this fingerprinting, samples were analyzed using single crystal X-ray diffraction (SC-XRD), Inductively Coupled Plasma Mass and Optical Emission Spectrometry (ICP-MS and ICP-OES), powder X-ray diffraction (P-XRD) and Raman Spectroscopy. The details of those analyses are given here.

2.2. SC-XRD

A single crystal from each wolframite sample was used for data collection on a Bruker ApexII diffractometer using graphite-monochromatized Mo Kα radiation; data collection parameters were identical for each crystal. The Bruker ApexII software package was used for processing of the structure data, structure solution and refinement. The structures were solved by direct methods; SHELXL-97 software (Sheldrick 2008) was used, with neutral atom scattering factors, for the refinement of the structures. These analysis were carried out at The University of Vermont.

2.3 ICP-MS and ICP-OES

Sample material was crushed and handpicked to remove foreign grains from each specimen and ensure purity for chemical analysis, which was performed on a Varian 820 ICP-MS using a standard addition method for the trace elements and an Agilent 720ES ICP-OES using external standards for the major elements. Approximately 9.3 mg of sample material was reacted in a teflon Savillex beaker with aqua regia on a hotplate for two days at 100° C to dissolve the mineral, which was then dried, transferred to weighing paper, and mixed with 50 mg lithium metaborate and 50 mg lithium carbonate. The mixture was fused in a graphite crucible at 950° C for 20 minutes, and then transferred to a LDPE plastic bottle containing 100 ml of 1% (0.29N) nitric acid and 1 ml of hydrogen peroxide and 10 µl phosphoric acid. Major elements were analyzed using a 1:15 dilution. These analyses were carried out at Miami University by Dr. John P. Morton.

2.4. P-XRD

The remaining wolframite samples were powdered under acetone by hand with an agate mortar and pestle and mounted in a 0.5 mm well glass slide for data collection on a Rigaku MiniFlexII Desktop X-ray diffractometer using graphite-monochromatized Cu Kα radiation. Rigaku's PDXL software package was used for phase identification and quantification and Rietveld refinement. Details of the data collection including running parameters, and phase data are as follows: Rietveld range was 13–70° 2θ, 0.02° steps, 5 seconds per step measurement axis with a tube voltage of 30 kV and tube current of 15 mA for both runs types for all samples.

2.5. Raman Spectroscopy

Sample material that had been set aside initially were used for Raman spectroscopy (method outlined by Smith and Dent 2005), which was conducted at Miami University's Molecular Microspectroscopy Lab by John Rakovan. A Renishaw inVia Raman Microscope used two lasers to collect spectra, often at varying powers. The samples were mounted as smear slides, suspended in acetone and dripped on to a glass microscope slide using a pipette in preparation for analysis. Some sample was analyzed as a powder whereas other spectra were gathered form a single crystal whose orientation to the lasers was measured vertically, perpendicular to the cleavage surface as well as on the terminated surface.

2.6. Data Analysis

Two statistical methods were used for analyzing the four groups of data described above: Ward's method of Hierarchal Clustering, and Linear, Common Covariance Discriminate Analysis. The JMP statistical software package was used to generate dendrograms for each type of analysis. Clustering analysis assumes that there are no nominal data available, only continuous information for each sample, whereas discriminate analyses uses nominal data in a predictive manor to attempt to classify samples into categories based on the given criteria. Clustering analysis groups like samples together with no prior information as to which categories into which they fit. By characterizing data and putting each individual data point in space into proper categories, the goal of linear common covariance is to develop a function that can effectively classify the samples in this study and also be usable outside of the scope of this study to correctly predict what group a sample will fall into. Using these statistical analyses to determine relationships within the data, it was possible to determine that fingerprinting the mineral wolframite can be done to a certain extent using the methods outlined above. Certain data sets were more effective in fingerprinting than others, which will be discussed further in the results section.

CHAPTER 3: RESULTS

3.1. SC-XRD

Prior to this work, only structures of end-member or near-end-member samples of ferberite or hübnerite have been published; the American Mineralogist Crystal Structure Database lists two "light ferberite" structures (Escobar 1971), as well as one other (Ulku 1967). The hübnerite crystal structure was also published the same year (Dachs 1967). Five synthetic high pressure hübnerite structures were later published as well (Macavei 1993). Tables 3-1 and 3-2 show all of the crystal structure data that have been gathered for ferberites and hübnerites within these studies.

Table 3-1. Previous Ferberite Atomic Data from The American Mineralogist Crystal Structure Database

		Escobar 1	Escobar 2	Ulku
W	x	0	0	0
	y	0.1808	0.1808	0.1799
	z	¼	¼	¼
Fe	x	½	½	½
	y	0.3215	0.3125	0.6744
	z	¾	¾	¼
O1	x	0.2167	0.2158	0.2159
	y	0.1017	0.1068	0.1050
	z	0.5833	0.5833	0.566
O2	x	0.2583	0.2623	0.2538
	y	0.3900	0.3850	0.3744
	z	0.0900	0.0912	0.1096
Unit Cell	*a*	4.753	4.750	4.730
	b	5.720	5.720	5.703
	c	4.968	4.970	4.952
	β	90.08	90.17	90.00

Table 3-2. Previous Hübnerite Atomic Data from The American Mineralogist Crystal Structure Database

		Dachs	Macavei1*	Macavei2**	Macavei3	Macavei4	Macavei5
W	x	0	0	0	0	0	0
	y	0.1815	0.1800	0.1800	0.1811	0.1815	0.1821
	z	¼	¼	¼	¼	¼	¼
Mn	x	½	½	½	½	½	½
	y	0.6804	0.6849	0.6849	0.6849	0.6870	0.6853
	z	¼	¼	¼	¼	¼	¼
O1	x	0.2100	0.2110	0.2110	0.2130	0.2100	0.2130
	y	0.0987	0.1020	0.1020	0.1020	0.1070	0.1060
	z	0.5568	0.9430	0.9410	0.9430	0.9410	0.9420
O2	x	0.2528	0.2500	0.2500	0.2500	0.2510	0.2500
	y	0.3776	0.3740	0.3750	0.3760	0.3810	0.3810
	z	0.1080	0.3930	0.3920	0.3940	0.3920	0.3920
Unit Cell	*a*	4.820	4.830	4.827	4.789	4.776	4.762
	b	5.760	5.760	5.761	5.711	5.681	5.660
	c	4.970	4.994	4.997	4.974	4.961	4.951
	β	89.12	91.14	91.14	91.22	91.19	91.23

* In open air
** In diamond anvil cell

Based on these data, the range of crystallographic and structural properties for the wolframite solid solution was not known. Below we summarize the results of crystal structure studies from 14 samples along the wolframite solid solution series. Details of the data collection, crystal data, structure solution and refinements are given in Tables

3-3 through 3-16.

Table 3-3. Sample and Crystal Data SAX

Unit cell dimensions	a = 4.7931(9) Å b = 5.7397(11) Å β = 90.711(2)° c = 4.9911(9) Å
Theta range for data collection	3.55 to 29.98°
Index ranges	-6<=h<=6, -8<=k<=8, -7<=l<=7
Reflections collected	2500
Independent reflections	404 [R(int) = 0.0191]
Structure solution program	SHELXS-97 (Sheldrick, 2008)
Refinement method	Full-matrix least-squares on F^2
Function minimized	$\Sigma\, w(F_o^2 - F_c^2)^2$
Data / restraints / parameters	404 / 0 / 31
Goodness-of-fit on F^2	0.532
Δ/σ_{max}	0.000
Final R indices	404 data; I>2σ(I) R1 = 0.0115, wR2 = 0.0379 all data R1 = 0.0115, wR2 = 0.0379
Weighting scheme	$w=1/[\sigma^2(F_o^2)+(0.0620P)^2+2.2517P]$ where $P=(F_o^2+2F_c^2)/3$
Largest diff. peak and hole	1.655 and -1.073 eÅ^{-3}

Table 3-4. Sample and Crystal Data USA1

Unit cell dimensions	a = 4.827(2) Å b = 5.758(2) Å β = 91.043(6)° c = 5.004(2) Å
Theta range for data collection	3.54 to 29.95°
Index ranges	-6<=h<=6, -8<=k<=6, -6<=l<=6
Reflections collected	1589
Independent reflections	405 [R(int) = 0.0149]
Structure solution program	SHELXS-97 (Sheldrick, 2008)
Refinement method	Full-matrix least-squares on F^2
Function minimized	$\Sigma\, w(F_o^2 - F_c^2)^2$
Data / restraints / parameters	405 / 0 / 31
Goodness-of-fit on F^2	1.141
Δ/σ_{max}	0.001
Final R indices	398 data; I>2σ(I) R1 = 0.0205, wR2 = 0.0547 all data R1 = 0.0210, wR2 = 0.0549
Weighting scheme	$w=1/[\sigma^2(F_o^2)+(0.0416P)^2+0.5504P]$ where $P=(F_o^2+2F_c^2)/3$
Largest diff. peak and hole	3.143 and -2.932 eÅ^{-3}

Table 3-5. Sample and Crystal Data 90,695 (AUS1)

Unit cell dimensions	a = 4.7514(6) Å b = 5.7198(7) Å β = 90.124(2)° c = 4.9720(6) Å
Theta range for data collection	3.56 to 29.95°
Index ranges	-6<=h<=6, -8<=k<=8, -6<=l<=6
Reflections collected	2448
Independent reflections	398 [R(int) = 0.0293]
Structure solution program	SHELXS-97 (Sheldrick, 2008)
Refinement method	Full-matrix least-squares on F^2
Function minimized	$\Sigma\, w(F_o^2 - F_c^2)^2$
Data / restraints / parameters	398 / 0 / 30
Goodness-of-fit on F^2	1.358
Δ/σ_{max}	0.001
Final R indices	398 data; I>2σ(I) R1 = 0.0147, wR2 = 0.0403 all data R1 = 0.0147, wR2 = 0.0403
Weighting scheme	$w=1/[\sigma^2(F_o^2)+(0.0204P)^2+0.2810P]$ where $P=(F_o^2+2F_c^2)/3$
Largest diff. peak and hole	1.494 and -1.797 eÅ^{-3}

Table 3-6. Sample and Crystal Data POR

Unit cell dimensions	a = 4.755(4) Å b = 5.732(5) Å β = 90.008(11)° c = 4.978(4) Å
Theta range for data collection	3.55 to 29.94°
Index ranges	-6<=h<=6, -7<=k<=8, -7<=l<=6
Reflections collected	2159
Independent reflections	378 [R(int) = 0.0553]
Structure solution program	SHELXS-97 (Sheldrick, 2008)
Refinement method	Full-matrix least-squares on F^2
Function minimized	$\Sigma\, w(F_o^2 - F_c^2)^2$
Data / restraints / parameters	378 / 0 / 31
Goodness-of-fit on F^2	1.065
Δ/σ_{max}	0.000
Final R indices	374 dataI>2σ(I) R1 = 0.0239, wR2 = 0.0604 all data R1 = 0.0242, wR2 = 0.0607
Weighting scheme	$w=1/[\sigma^2(F_o^2)+(0.0368P)^2+1.5703P]$ where $P=(F_o^2+2F_c^2)/3$
Largest diff. peak and hole	2.999 and -2.997 eÅ^{-3}

Table 3-7. Sample and Crystal Data BOL

Unit cell dimensions	a = 4.7446(6) Å b = 5.7147(7) Å β = 90.054(2)° c = 4.9701(6) Å
Theta range for data collection	3.57 to 29.99°
Index ranges	-6<=h<=6, -8<=k<=8, -6<=l<=6
Reflections collected	2378
Independent reflections	399 [R(int) = 0.0347]
Structure solution program	SHELXS-97 (Sheldrick, 2008)
Refinement method	Full-matrix least-squares on F^2
Function minimized	$\Sigma\, w(F_o^2 - F_c^2)^2$
Data / restraints / parameters	399 / 0 / 31
Goodness-of-fit on F^2	1.217
Δ/σ_{max}	0.000
Final R indices	399 data; I>2σ(I) R1 = 0.0168, wR2 = 0.0439 all data R1 = 0.0168, wR2 = 0.0439
Weighting scheme	$w=1/[\sigma^2(F_o^2)+(0.0238P)^2+0.5868P]$ where $P=(F_o^2+2F_c^2)/3$
Largest diff. peak and hole	1.724 and -2.025 eÅ^{-3}

Table 3-8. Sample and Crystal Data AUS2

Unit cell dimensions	a = 4.7653(10) Å b = 5.7264(12) Å β = 90.324(2)° c = 4.9778(11) Å
Theta range for data collection	3.56 to 29.99°
Index ranges	-6<=h<=6, -8<=k<=8, -7<=l<=7
Reflections collected	2268
Independent reflections	401 [R(int) = 0.0284]
Structure solution program	SHELXS-97 (Sheldrick, 2008)
Refinement method	Full-matrix least-squares on F^2
Function minimized	$\Sigma\, w(F_o^2 - F_c^2)^2$
Data / restraints / parameters	401 / 0 / 31
Goodness-of-fit on F^2	1.093
Δ/σ_{max}	3.824
Final R indices	401 data; I>2σ(I) R1 = 0.0166, wR2 = 0.0419 all data R1 = 0.0166, wR2 = 0.0419
Weighting scheme	$w=1/[\sigma^2(F_o^2)+(0.0249P)^2+1.2040P]$ where $P=(F_o^2+2F_c^2)/3$
Largest diff. peak and hole	4.867 and -1.549 eÅ^{-3}

Table 3-9. Sample and Crystal Data USA2

Unit cell dimensions	a = 4.8197(13) Å b = 5.7586(15) Å β = 91.080(3)° c = 5.0012(13) Å
Theta range for data collection	3.54 to 29.97°
Index ranges	-6<=h<=6, -8<=k<=8, -7<=l<=7
Reflections collected	2506
Independent reflections	408 [R(int) = 0.0219]
Structure solution program	SHELXS-97 (Sheldrick, 2008)
Refinement method	Full-matrix least-squares on F^2
Function minimized	$\Sigma\, w(F_o^2 - F_c^2)^2$
Data / restraints / parameters	408 / 0 / 31
Goodness-of-fit on F^2	1.138
Δ/σ_{max}	0.001
Final R indices	405 data; I>2σ(I) R1 = 0.0177, wR2 = 0.0467 all data R1 = 0.0178, wR2 = 0.0468
Weighting scheme	$w=1/[\sigma^2(F_o^2)+(0.0345P)^2+0.4393P]$ where $P=(F_o^2+2F_c^2)/3$
Largest diff. peak and hole	2.479 and -2.246 eÅ^{-3}

Table 3-10. Sample and Crystal Data USA3

Unit cell dimensions	a = 4.7542(12) Å b = 5.7238(15) Å β = 90.174(3)° c = 4.9728(13) Å
Theta range for data collection	3.56 to 29.93°
Index ranges	-6<=h<=6, -8<=k<=8, -6<=l<=6
Reflections collected	1905
Independent reflections	398 [R(int) = 0.0416]
Structure solution program	SHELXS-97 (Sheldrick, 2008)
Refinement method	Full-matrix least-squares on F^2
Function minimized	$\Sigma\, w(F_o^2 - F_c^2)^2$
Data / restraints / parameters	398 / 0 / 31
Goodness-of-fit on F^2	1.182
Δ/σ_{max}	1.438
Final R indices	397 data; I>2σ(I) R1 = 0.0300, wR2 = 0.0765 all data R1 = 0.0301, wR2 = 0.0766
Weighting scheme	$w=1/[\sigma^2(F_o^2)+(0.0537P)^2+0.8901P]$ where $P=(F_o^2+2F_c^2)/3$
Largest diff. peak and hole	3.411 and -6.334 eÅ^{-3}

Table 3-11. Sample and Crystal Data ENG

Unit cell dimensions	a = 4.7858(11) Å b = 5.7378(13) Å β = 90.324(2)° c = 4.9862(11) Å
Theta range for data collection	3.55 to 29.99°
Index ranges	-6<=h<=6, -8<=k<=8, -6<=l<=6
Reflections collected	2433
Independent reflections	404 [R(int) = 0.0418]
Structure solution program	SHELXS-97 (Sheldrick, 2008)
Refinement method	Full-matrix least-squares on F^2
Function minimized	$\Sigma\, w(F_o^2 - F_c^2)^2$
Data / restraints / parameters	404 / 0 / 31
Goodness-of-fit on F^2	1.175
Δ/σ_{max}	0.001
Final R indices	403 data; I>2σ(I) R1 = 0.0166, wR2 = 0.0419 all data R1 = 0.0166, wR2 = 0.0419
Weighting scheme	$w=1/[\sigma^2(F_o^2)+(0.0210P)^2+1.1844P]$ where $P=(F_o^2+2F_c^2)/3$
Largest diff. peak and hole	1.868 and -2.570 eÅ^{-3}

Table 3-12. Sample and Crystal Data BOH

Unit cell dimensions	a = 4.7465(14) Å b = 5.7179(17) Å β = 90.213(3)° c = 4.9653(14) Å
Theta range for data collection	3.56 to 29.97°
Index ranges	-6<=h<=6, -8<=k<=8, -6<=l<=6
Reflections collected	2432
Independent reflections	399 [R(int) = 0.0251]
Structure solution program	SHELXS-97 (Sheldrick, 2008)
Refinement method	Full-matrix least-squares on F^2
Function minimized	$\Sigma\, w(F_o^2 - F_c^2)^2$
Data / restraints / parameters	399 / 0 / 31
Goodness-of-fit on F^2	1.229
Δ/σ_{max}	0.000
Final R indices	398 data; I>2σ(I) R1 = 0.0177, wR2 = 0.0481 all data R1 = 0.0177, wR2 = 0.0481
Weighting scheme	$w=1/[\sigma^2(F_o^2)+(0.0304P)^2+0.8153P]$ where $P=(F_o^2+2F_c^2)/3$
Largest diff. peak and hole	2.727 and -3.290 eÅ^{-3}

Table 3-13. Sample and Crystal Data USA4

Unit cell dimensions	a = 4.8074(8) Å b = 5.7518(10) Å β = 90.892(2)° c = 4.9973(9) Å
Theta range for data collection	3.54 to 29.98°
Index ranges	-6<=h<=6, -8<=k<=8, -7<=l<=6
Reflections collected	2481
Independent reflections	407 [R(int) = 0.0326]
Structure solution program	SHELXS-97 (Sheldrick, 2008)
Refinement method	Full-matrix least-squares on F^2
Function minimized	$\Sigma\, w(F_o^2 - F_c^2)^2$
Data / restraints / parameters	407 / 0 / 31
Goodness-of-fit on F^2	1.259
Δ/σ_{max}	0.000
Final R indices	407 data; I>2σ(I) R1 = 0.0177, wR2 = 0.0440 all data R1 = 0.0177, wR2 = 0.0440
Weighting scheme	$w=1/[\sigma^2(F_o^2)+(0.0204P)^2+1.2120P]$ where $P=(F_o^2+2F_c^2)/3$
Largest diff. peak and hole	2.461 and -3.171 eÅ^{-3}

Table 3-14. Sample and Crystal Data CR

Unit cell dimensions	a = 4.7927(14) Å b = 5.7340(17) Å β = 90.701(4)° c = 4.9892(15) Å
Theta range for data collection	3.55 to 29.99°
Index ranges	-6<=h<=6, -8<=k<=7, -7<=l<=7
Reflections collected	2084
Independent reflections	404 [R(int) = 0.0146]
Structure solution program	SHELXS-97 (Sheldrick, 2008)
Refinement method	Full-matrix least-squares on F^2
Function minimized	$\Sigma\, w(F_o^2 - F_c^2)^2$
Data / restraints / parameters	404 / 0 / 30
Goodness-of-fit on F^2	1.131
Δ/σ_{max}	0.000
Final R indices	397 data; I>2σ(I) R1 = 0.0131, wR2 = 0.0319 all data R1 = 0.0137, wR2 = 0.0321
Weighting scheme	$w=1/[\sigma^2(F_o^2)+(0.0192P)^2+0.7043P]$ where $P=(F_o^2+2F_c^2)/3$
Largest diff. peak and hole	0.983 and -1.878 eÅ^{-3}

Table 3-15. Sample and Crystal Data PER

Unit cell dimensions	a = 4.7709(8) Å b = 5.7261(9) Å β = 90.369(2)° c = 4.9806(8) Å
Theta range for data collection	3.56 to 29.99°
Index ranges	-6<=h<=6, -8<=k<=8, -6<=l<=7
Reflections collected	2406
Independent reflections	398 [R(int) = 0.0308]
Structure solution program	SHELXS-97 (Sheldrick, 2008)
Refinement method	Full-matrix least-squares on F^2
Function minimized	$\Sigma\, w(F_o^2 - F_c^2)^2$
Data / restraints / parameters	398 / 0 / 31
Goodness-of-fit on F^2	1.182
Δ/σ_{max}	0.945
Final R indices	398 data; I>2σ(I) R1 = 0.0184, wR2 = 0.0474 all data R1 = 0.0184, wR2 = 0.0474
Weighting scheme	$w=1/[\sigma^2(F_o^2)+(0.0272P)^2+0.9652P]$ where $P=(F_o^2+2F_c^2)/3$
Largest diff. peak and hole	2.501 and -2.446 eÅ^{-3}

Table 3-16. Sample and Crystal Data KOR

Unit cell dimensions	a = 4.7678(10) Å b = 5.7348(11) Å β = 90.39(3)° c = 4.9853(10) Å
Theta range for data collection	3.55 to 29.97°
Index ranges	-6<=h<=6, -8<=k<=8, -7<=l<=7
Reflections collected	2448
Independent reflections	403 [R(int) = 0.0292]
Structure solution program	SHELXS-97 (Sheldrick, 2008)
Refinement method	Full-matrix least-squares on F^2
Function minimized	$\Sigma\, w(F_o^2 - F_c^2)^2$
Data / restraints / parameters	403 / 0 / 31
Goodness-of-fit on F^2	1.250
Δ/σ_{max}	0.000
Final R indices	403 data; I>2σ(I) R1 = 0.0138, wR2 = 0.0351 all data R1 = 0.0138, wR2 = 0.0351
Weighting scheme	$w=1/[\sigma^2(F_o^2)+(0.0138P)^2+0.7166P]$ where $P=(F_o^2+2F_c^2)/3$
Largest diff. peak and hole	1.125 and -1.569 eÅ^{-3}

Final atom coordinates and equivalent isotropic temperature factors are in Table 3-17.

Table 3-17. Atomic Coordinates Equivalent Isotropic Atomic Displacement Parameters (Å2)

Sample	atom	x/a	y/b	z/c	U(eq)	Occ.
SAX	W	1/2	0.68003(3)	1/4	0.00385(13)	$W_{1.00}$
USA1	W	1/2	0.68015(3)	1/4	0.00560(6)	$W_{1.00}$
AUS1	W	1/2	0.68013(3)	1/4	0.00311(9)	$W_{1.00}$
POR	W	1/2	0.67994(6)	1/4	0.0040(2)	$W_{1.00}$
BOL	W	1/2	0.68027(4)	1/4	0.00433(15)	$W_{1.00}$
AUS2	W	1/2	0.68013(5)	1/4	0.00470(17)	$W_{1.00}$
USA2	W	1/2	0.67988(4)	1/4	0.00609(15)	$W_{1.00}$
USA3	W	1/2	0.68021(6)	1/4	0.0040(3)	$W_{1.00}$
ENG	W	1/2	0.68016(4)	1/4	0.00148(16)	$W_{1.00}$
BOH	W	1/2	0.68027(4)	1/4	0.00190(16)	$W_{1.00}$
USA4	W	1/2	0.67998(4)	1/4	-0.00068(16)	$W_{1.00}$
CR	W	1/2	0.67985(4)	1/4	0.00469(8)	$W_{1.00}$
PER	W	1/2	0.68014(4)	1/4	0.00518(17)	$W_{1.00}$
KOR	W	1/2	0.67999(3)	1/4	0.00177(13)	$W_{1.00}$
SAX	Fe/Mn	0	0.18025(12)	1/4	0.0071(4)	$Mn_{0.04}Fe_{0.96}$
USA1	Fe/Mn	0	0.18486(14)	1/4	0.0091(2)	$Mn_{0.72}Fe_{0.28}$
AUS1	Fe/Mn	0	0.17446(12)	1/4	0.00346(19)	$Mn_{1.00}$
POR	Fe/Mn	0	0.1737(2)	1/4	0.0073(7)	$Mn_{1.00}$
BOL	Fe/Mn	0	0.17385(15)	1/4	0.0071(4)	$Mn_{0.40}Fe_{0.60}$
AUS2	Fe/Mn	0	0.17693(17)	1/4	0.0080(5)	$Mn_{0.50}Fe_{0.50}$
USA2	Fe/Mn	0	0.18365(16)	1/4	0.0091(5)	$Mn_{0.32}Fe_{0.68}$
USA3	Fe/Mn	0	0.1753(2)	1/4	0.0068(7)	$Mn_{0.36}Fe_{0.64}$
ENG	Fe/Mn	0	0.17890(17)	1/4	0.0046(5)	$Mn_{0.16}Fe_{0.84}$
BOH	Fe/Mn	0	0.17462(17)	1/4	0.0045(5)	$Mn_{0.54}Fe_{0.46}$
USA4	Fe/Mn	0	0.18163(17)	1/4	0.0022(4)	$Mn_{0.20}Fe_{0.80}$
CR	Fe/Mn	0	0.18022(14)	1/4	0.0075(3)	$Mn_{0.32}Fe_{0.68}$
PER	Fe/Mn	0	0.17710(18)	1/4	0.0085(5)	$Mn_{0.13}Fe_{0.87}$
KOR	Fe/Mn	0	0.17694(14)	1/4	0.0052(4)	$Fe_{1.00}$
SAX	O1	0.2885(6)	0.3963(5)	0.0608(5)	0.0070(5)	$O_{1.00}$
USA1	O1	0.2893(6)	0.3973(6)	0.0577(6)	0.0082(6)	$O_{1.00}$
AUS1	O1	0.2863(6)	0.3949(5)	0.0652(6)	0.0058(5)	$O_{1.00}$
POR	O1	0.7516(12)	0.8742(10)	0.1045(11)	0.0092(10)	$O_{1.00}$
BOL	O1	0.2859(7)	0.3942(6)	0.0656(7)	0.0070(6)	$O_{1.00}$
AUS2	O1	0.2868(9)	0.3954(7)	0.0631(8)	0.0079(7)	$O_{1.00}$
USA2	O1	0.2894(7)	0.3979(7)	0.0580(7)	0.0089(6)	$O_{1.00}$
USA3	O1	0.2858(12)	0.3954(11)	0.0649(11)	0.0071(10)	$O_{1.00}$
ENG	O1	0.2875(8)	0.3960(7)	0.0617(7)	0.0052(7)	$O_{1.00}$
BOH	O1	0.2858(8)	0.3945(7)	0.0641(7)	0.0039(6)	$O_{1.00}$
USA4	O1	0.2888(8)	0.3974(7)	0.0595(7)	0.0026(7)	$O_{1.00}$
CR	O1	0.2876(6)	0.3959(5)	0.0603(6)	0.0081(5)	$O_{1.00}$
PER	O1	0.2876(8)	0.3953(7)	0.0629(8)	0.0082(7)	$O_{1.00}$
KOR	O1	0.2869(6)	0.3954(5)	0.0625(6)	0.0042(5)	$O_{1.00}$
SAX	O2	0.2485(6)	0.8750(6)	0.1067(6)	0.0079(5)	$O_{1.00}$
USA1	O2	0.2491(6)	0.8756(6)	0.1064(6)	0.0104(6)	$O_{1.00}$
AUS1	O2	0.2478(6)	0.8753(6)	0.1055(6)	0.0060(5)	$O_{1.00}$
POR	O2	0.7150(11)	0.3926(10)	0.0653(11)	0.0097(10)	$O_{1.00}$
BOL	O2	0.2475(7)	0.8756(7)	0.1051(7)	0.0075(6)	$O_{1.00}$
AUS2	O2	0.2474(9)	0.8755(8)	0.1062(9)	0.0080(7)	$O_{1.00}$
USA2	O2	0.2481(8)	0.8751(7)	0.1065(7)	0.0098(6)	$O_{1.00}$
USA3	O2	0.2471(12)	0.8754(12)	0.1053(12)	0.0074(10)	$O_{1.00}$
ENG	O2	0.2468(8)	0.8748(7)	0.1061(8)	0.0050(7)	$O_{1.00}$
BOH	O2	0.2469(8)	0.8756(7)	0.1052(8)	0.0048(7)	$O_{1.00}$
USA4	O2	0.2484(8)	0.8743(7)	0.1065(8)	0.0035(7)	$O_{1.00}$
CR	O2	0.2482(6)	0.8750(5)	0.1068(6)	0.0083(5)	$O_{1.00}$
PER	O2	0.2476(8)	0.8748(8)	0.1053(8)	0.0091(7)	$O_{1.00}$
KOR	O2	0.2475(6)	0.8744(6)	0.1056(6)	0.0048(5)	$O_{1.00}$

For bond distances and bond-valence values for the 14 samples see Table 3-18.

Table 3-18. Select Bond Distances *d* in (Å) and Bond Valence Values (vu)

SAX		*d*	*vu*			*d*	*vu*
W-	O2(x2)	1.787(3)	1.44	$Mn_{0.04}Fe_{0.96}$	O1(x2)	2.092(3)	0.38
	O1(x2)	1.914(3)	1.02		O2(x2)	2.153(3)	0.32
	O1'(x2)	2.133(3)	0.56		O2'(x2)	2.241(3)	0.25
Mean, sum:		1.945	6.04			2.162	1.90
USA1		*d*	*vu*			*d*	*vu*
W-	O2(x2)	1.794(3)	1.41	$Mn_{0.72}Fe_{0.28}$	O1(x2)	2.103(3)	0.41
	O1(x2)	1.913(3)	1.02		O2(x2)	2.161(3)	0.35
	O1'(x2)	2.139(3)	0.55		O2'(x2)	2.273(3)	0.26
Mean, sum:		1.949	5.96			2.179	2.04
AUS1		*d*	*vu*			*d*	*vu*
W-	O2(x2)	1.787(3)	1.43	$Mn_{1.00}$	O1(x2)	2.071(3)	0.47
	O1(x2)	1.918(3)	1.01		O2(x2)	2.141(3)	0.39
	O1'(x2)	2.129(3)	0.57		O2'(x2)	2.199(3)	0.33
Mean, sum:		1.945	6.02			2.137	2.38
POR		*d*	*vu*			*d*	*vu*
W-	O2(x2)	1.788(5)	1.43	$Mn_{1.00}$	O1(x2)	2.063(5)	0.48
	O1(x2)	1.919(5)	1.01		O2(x2)	2.141(5)	0.39
	O1'(x2)	2.145(5)	0.55		O2'(x2)	2.206(5)	0.33
Mean, sum:		1.951	5.98			2.136	2.40
BOL		*d*	*vu*			*d*	*vu*
W-	O2(x2)	1.788(4)	1.43	$Mn_{0.40}Fe_{0.60}$	O1(x2)	2.066(4)	0.43
	O1(x2)	1.917(3)	1.01		O2(x2)	2.138(4)	0.36
	O1'(x2)	2.131(4)	0.57		O2'(x2)	2.192(4)	0.31
Mean, sum:		1.945	6.02			2.132	2.20
AUS2		*d*	*vu*			*d*	*vu*
W-	O2(x2)	1.790(4)	1.42	$Mn_{0.50}Fe_{0.50}$	O1(x2)	2.077(4)	0.43
	O1(x2)	1.915(4)	1.02		O2(x2)	2.145(4)	0.36
	O1'(x2)	2.132(4)	0.57		O2'(x2)	2.212(4)	0.30
Mean, sum:		1.946	6.02			2.145	2.18
USA2		*d*	*vu*			*d*	*vu*
W-	O2(x2)	1.795(4)	1.41	$Mn_{0.32}Fe_{0.68}$	O1(x2)	2.107(4)	0.38
	O1(x2)	1.914(4)	1.02		O2(x2)	2.155(4)	0.34
	O1'(x2)	2.133(4)	0.56		O2'(x2)	2.266(4)	0.25
Mean, sum:		1.947	5.98			2.176	1.94

USA3		*d*	*vu*			*d*	*vu*
W-	O2(x2)	1.791(6)	1.42	$Mn_{0.36}Fe_{0.64}$	O1(x2)	2.071(6)	0.43
	O1(x2)	1.920(6)	1.00		O2(x2)	2.139(6)	0.35
	O1'(x2)	2.130(6)	0.57		O2'(x2)	2.202(6)	0.30
Mean, sum:		1.947	5.98			2.137	2.16
ENG		*d*	*vu*			*d*	*vu*
W-	O2(x2)	1.793(4)	1.41	$Mn_{0.16}Fe_{0.84}$	O1(x2)	2.086(4)	0.40
	O1(x2)	1.916(4)	1.01		O2(x2)	2.146(4)	0.34
	O1'(x2)	2.135(4)	0.56		O2'(x2)	2.230(4)	0.27
Mean, sum:		1.948	5.96			2.154	2.02
BOH		*d*	*vu*			*d*	*vu*
W-	O2(x2)	1.790(4)	1.42	$Mn_{0.54}Fe_{0.46}$	O1(x2)	2.070(4)	0.44
	O1(x2)	1.913(4)	1.02		O2(x2)	2.133(4)	0.37
	O1'(x2)	2.133(4)	0.56		O2'(x2)	2.195(4)	0.31
Mean, sum:		1.945	6.00			2.133	2.24
USA4		*d*	*vu*			*d*	*vu*
W-	O2(x2)	1.789(4)	1.43	$Mn_{0.20}Fe_{0.80}$	O1(x2)	2.101(4)	0.38
	O1(x2)	1.916(4)	1.01		O2(x2)	2.153(4)	0.33
	O1'(x2)	2.133(4)	0.56		O2'(x2)	2.257(4)	0.25
Mean, sum:		1.946	6.00			2.170	1.92
CR		*d*	*vu*			*d*	*vu*
W-	O2(x2)	1.788(3)	1.43	$Mn_{0.32}Fe_{0.68}$	O1(x2)	2.087(3)	0.40
	O1(x2)	1.913(3)	1.02		O2(x2)	2.153(3)	0.34
	O1'(x2)	2.135(3)	0.56		O2'(x2)	2.238(3)	0.27
Mean, sum:		1.945	6.02			2.159	2.02
PER		*d*	*vu*			*d*	*vu*
W-	O2(x2)	1.789(4)	1.43	$Mn_{0.13}Fe_{0.87}$	O1(x2)	2.081(4)	0.40
	O1(x2)	1.914(4)	1.02		O2(x2)	2.142(4)	0.34
	O1'(x2)	2.131(4)	0.56		O2'(x2)	2.218(4)	0.27
Mean, sum:		1.945	6.02			2.147	2.02
KOR		*d*	*vu*			*d*	*vu*
W-	O2(x2)	1.789(3)	1.43	$Fe_{1.00}$	O1(x2)	2.082(3)	0.39
	O1(x2)	1.915(3)	1.02		O2(x2)	2.142(3)	0.33
	O1'(x2)	2.134(3)	0.56		O2'(x2)	2.221(3)	0.27
Mean, sum:		1.946	6.02			2.148	1.98

In the case of the mineral wolframite, Mn^{2+} exists in the high spin state with a 0.83 Å ionic radius in six fold coordination, and Fe^{2+} in the high spin state with a 0.78 Å ionic radius in octahedral coordination (Bloss 1994). Because we find both of these elements in high spin states, as evidenced by their radii, Hund's rule of multiplicity must apply (Burns 1970).

Variability in terms of unit cell parameters for each of the 14 samples yielded a range of β values from 90.892(2)° to 90.008(11)°, as well as *a*, *b*, and *c* dimensions, all of which can be seen in Tables 3-16 to 3-3. Figures 3-1 through 3-4 elucidate the relationship between composition and unit-cell parameters for each of the 14 samples.

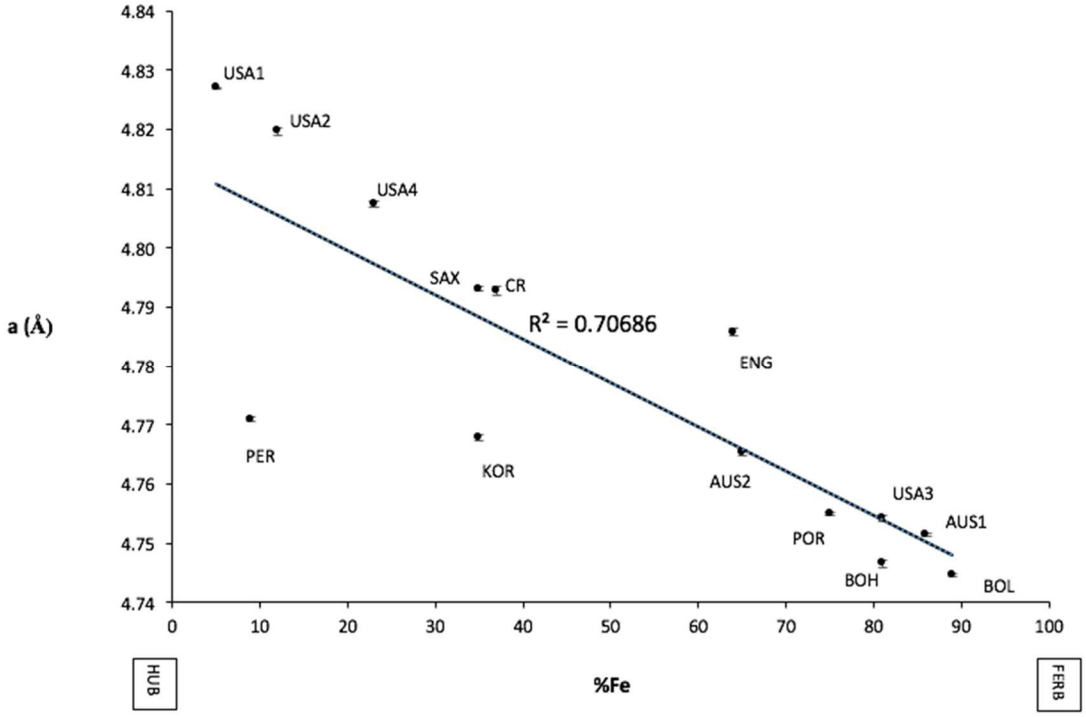

Figure 3-1. Composition versus Unit Cell Parameter a

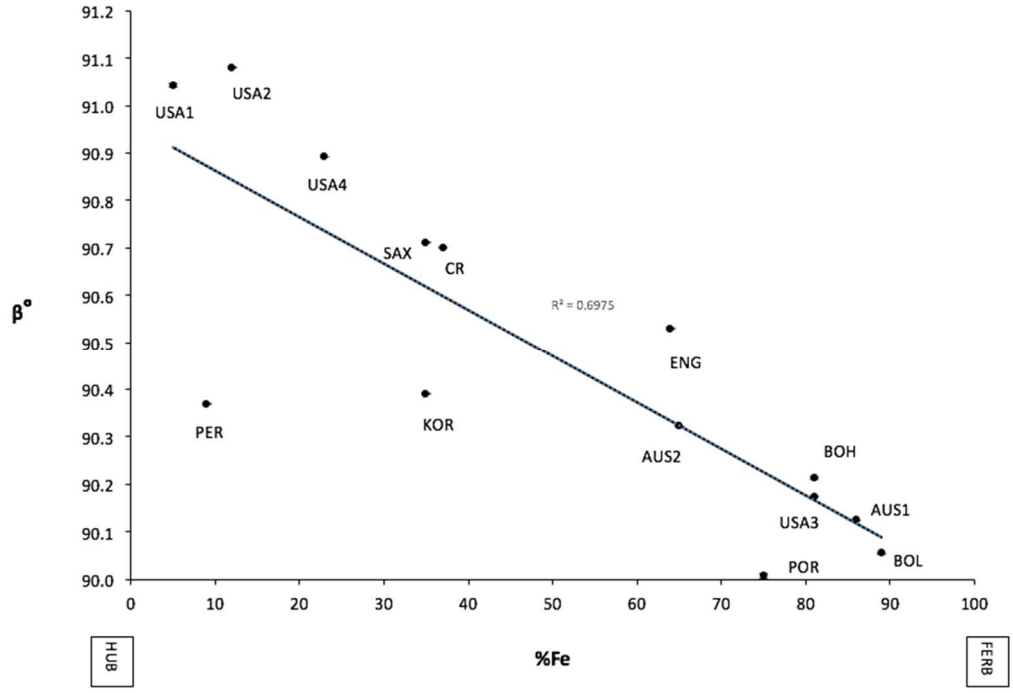

Figure 3-2. Composition versus Unit Cell Parameter

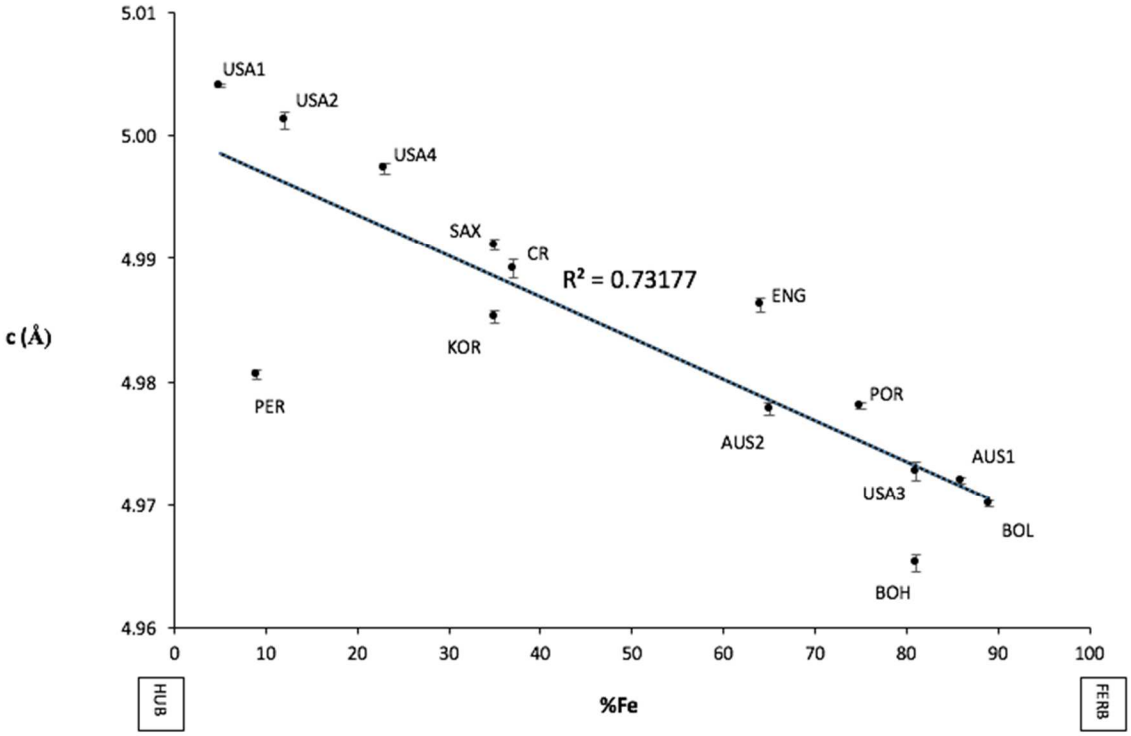

Figure 3-3. Composition versus Unit Cell Parameter *c*

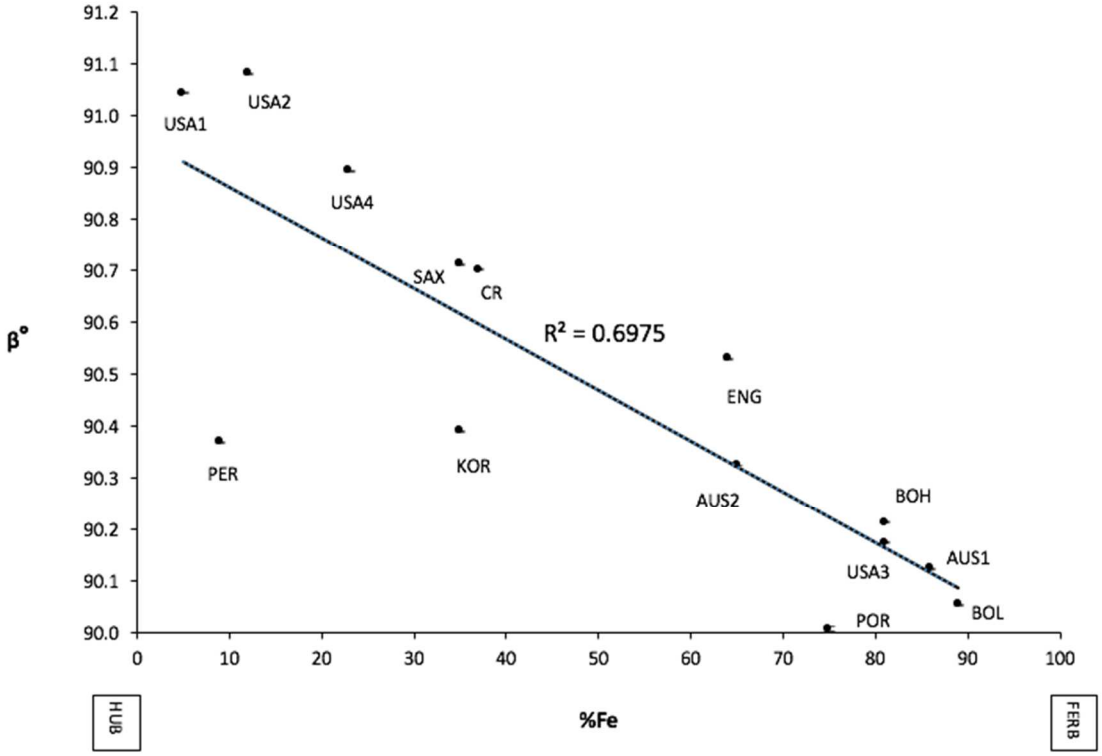

Figure 3-4. Composition versus Unit Cell Parameter β

Differences in the atomic positions will be manifested in differences in cation-anion bond distances. Considering the W-O_6 octahedron, the average W-O_6 bond distances can be found in Table 6. The greatest bond distance observed in sample USA2 between the W and O2 atom was 1.795(4) Å. The smallest bond distance observed in sample AUS1 between the W and O2 atom was 1.787(3) Å, a difference of 0.008. The greatest bond distance observed in sample USA3 between the W and O1 atom was 1.920(6) Å. The smallest bond distance observed in sample USA1 between the W and O1 atom was 1.913(3) Å, a difference of 0.007. The greatest bond distance observed in sample POR between the W and O1' atom was 2.145(5) Å. The smallest bond distance observed between the W and O1' atom was 2.129(3) Å AUS1, a difference of 0.016.

Figures 3-5 through 3-7 show the relationship between average Fe/Mn O1, O2, O2' bond distances and composition.

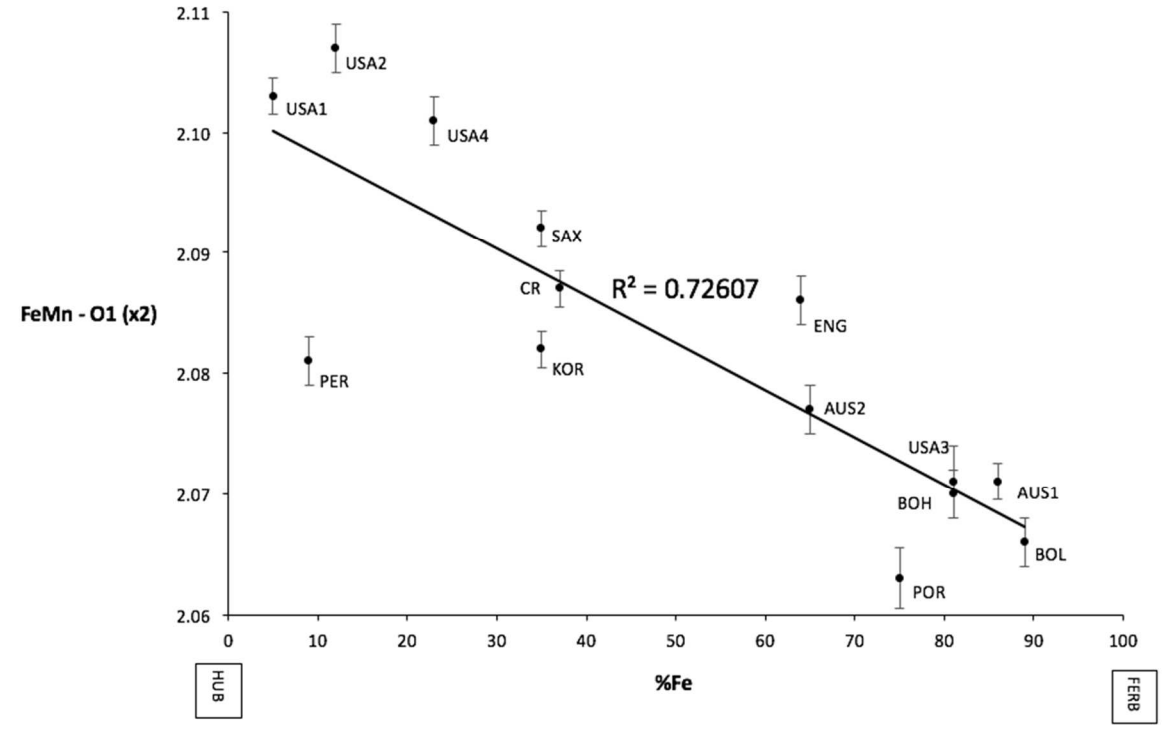

Figure 3-5. Composition versus Fe/Mn O1 Bond Distance

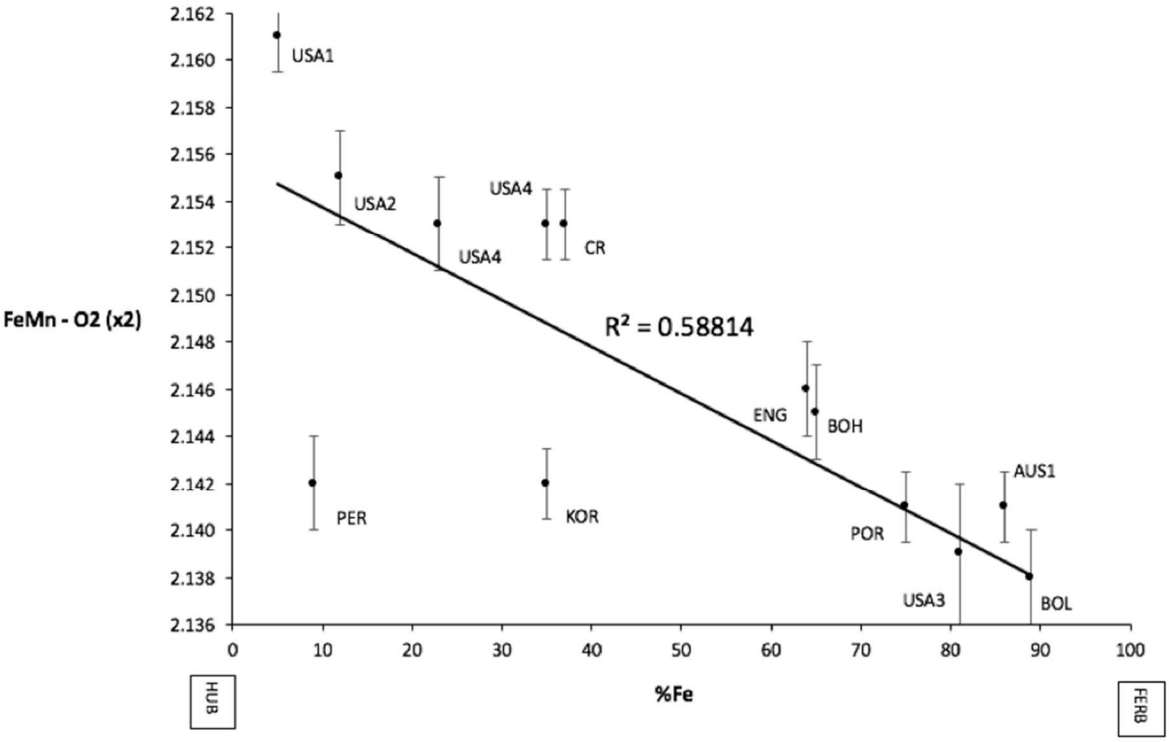

Figure 3-6. Composition versus Fe/Mn O2 Bond Distances

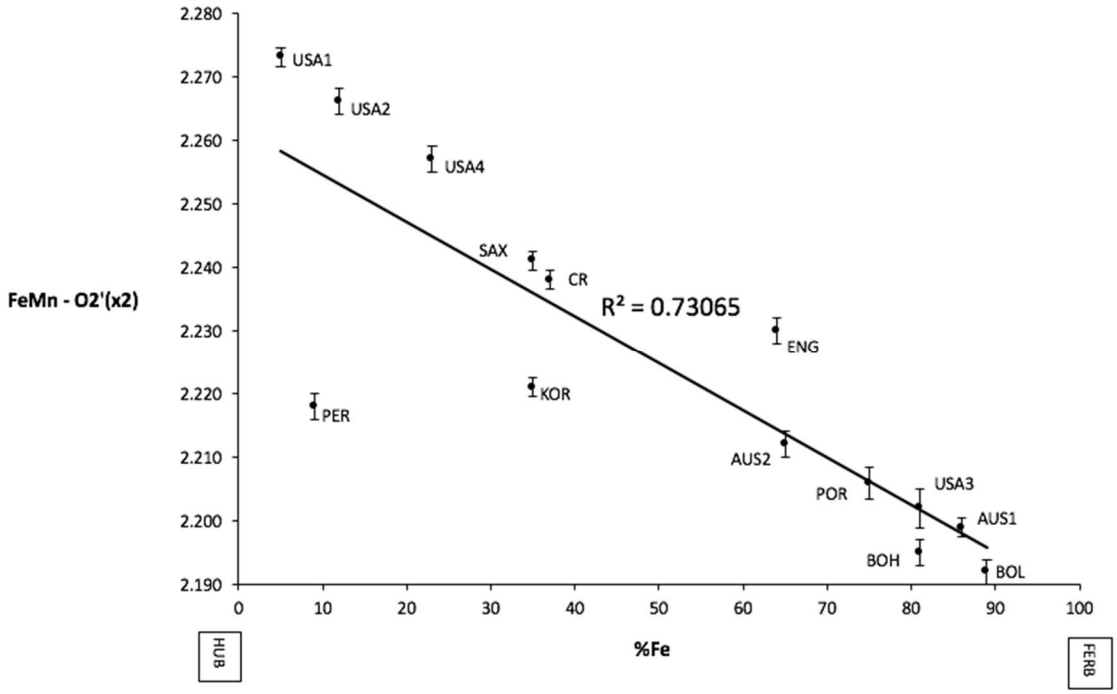

Figure 3-7. Composition versus Fe/Mn O2' Bond Distances

Single crystal data are not available for sample UGA. Unique in that it appears to be polycrystalline, a single grain could not be extracted for single crystal diffraction. Details will be elaborated in the discussion section to follow. The wolframite crystal structure is shown in Figure 3-8 below, which was generated using ATOMS 3D atomic modeling software. In the *c* direction, ribbons of iron-manganese octahedra are shown in gray, linked together by black tungsten octahedra and its bonds to oxygen.

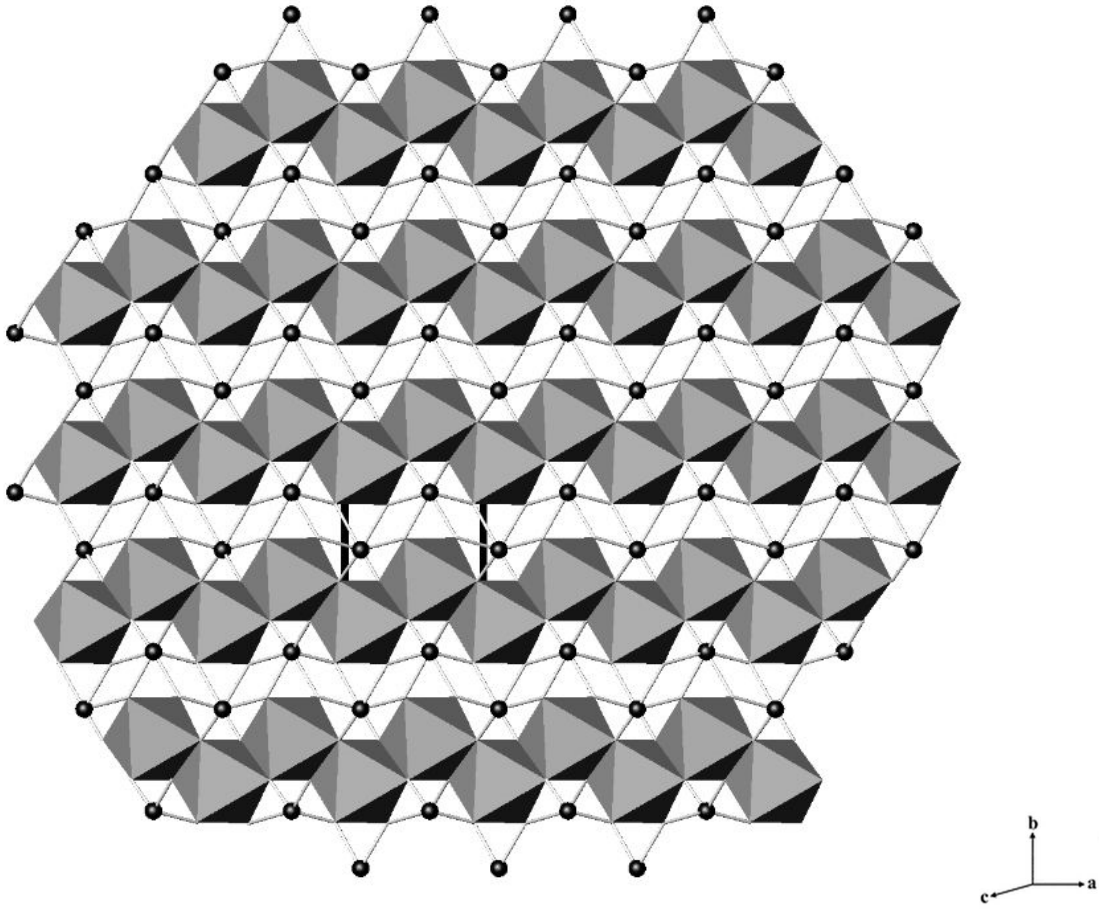

Figure 3-8. Wolframite Atomic Structure

3.2. ICP-MS/OES

The results of these analyses are given in Table 3-19, showing ICP-OES results, and Tables 3-20 through 3-22 give ICP-MS results. Major elements were analyzed by external standards on an Agilent 720ES ICP-OES using 5 ppm Rhodium as internal standard. Trace elements analyzed by standard addition on a Varian 820 ICP-MS using 100 ppb Rh and Re as internal standards. A sample (9.34 mg) was dissolved by a combination of acid dissolution and flux fusion in 100 ml of 1% HNO3.

Internal standards were added in constant amounts to the samples (standard addition) as well as the blank and calibration standard used. The ratio of the sample's signal against the internal standard signal were plotted as a function of the sample's standard concentration to aid in calibration. This ratio was then used to obtain sample concentrations from a calibration curve. These internal standards provided similar but distinguishable signals to that of the samples analyzed. Similarly, the external standard wasn't added to an unknown, but run independently, as its own sample at different concentrations to derive a standard curve (Oliveira 2010).

Table 3-19. Major Elemental Composition Analyzed by Agilent ICP-OES using external standards

Element (%oxide)	SAX	USA1	AUS1	POR	BOL	AUS2
FeO	8.11	1.17	19.81	18.83	20.90	14.71
MnO	13.18	21.33	3.61	7.99	2.03	7.89
SiO_2	0.73	0.76	2.05	0.92	0.69	2.47
WO_3	73.26	72.88	73.75	73.28	76.16	73.43
Sum (Major)	*95.28*	*96.14*	*99.22*	*101.02*	*99.78*	*98.50*
Sum (Major+Trace)	*99.50*	*97.14*	*101.42*	*102.28*	*100.82*	*100.19*

Element (%oxide)	USA2	USA3	UGA	ENG	BOH	USA4
FeO	2.65	21.18	25.31	14.82	19.05	5.32
MnO	21.51	4.36	0.75	8.39	3.42	17.72
SiO_2	1.08	0.69	0.98	0.69	0.68	0.74
WO_3	73.26	75.51	73.67	74.87	75.62	74.39
Sum (Major)	*98.50*	*101.74*	*100.71*	*98.77*	*98.77*	*98.17*
Sum (Major+Trace)	*100.33*	*102.53*	*101.72*	*99.58*	*100.35*	*99.80*

Element (%oxide)	CR	PER	KOR
FeO	8.58	2.07	8.21
MnO	14.60	20.72	14.90
SiO_2	0.68	0.74	0.71
WO_3	73.93	74.65	74.45
Sum (Major)	*97.79*	*98.18*	*98.27*
Sum (Major+Trace)	*100.06*	*98.81*	*99.51*

Table 3-20. Trace Elemental Composition Analyzed by Varian 820 ICP-MS using standard addition

Element (ppm)	SAX	USA1	AUS1	POR	BOL	AUS2
Be	0.0	0.0	0.1	0.3	0.0	0.0
Na*	14.9	216.2	858.2	182.0	51.8	27.3
Mg*	106.9	193.7	332.6	1121.3	2553.8	266.6
Al*	1924.5	1548.8	4231.4	2172.7	1954.7	1124.4
K*	0.0	40.9	2120.5	0.0	57.6	31.4
Ca*	14676.7	2452.3	1551.9	1408.9	705.1	5590.9
Sc	1642.8	143.7	579.4	1.8	6.9	209.9
Ti*	341.8	369.1	468.8	170.9	196.4	126.2
V	0.0	0.0	0.0	0.0	0.6	0.0
Cr	0.0	0.0	0.0	0.0	0.0	0.0
Co	0.6	0.9	1.3	1.4	7.3	1.9
Ni	7.1	20.9	13.9	8.1	18.1	5.0
Cu	5.5	4.8	2.3	26.9	8.3	1.9
Zn	77.3	232.1	75.6	75.8	58.3	51.2
Ga	12.6	19.6	4.4	7.0	2.6	8.9
Ge	7.4	11.6	3.4	5.1	2.8	6.8
As	75.7	27.3	32.0	28.2	41.1	23.8
Rb	0.6	0.3	4.4	1.8	0.4	0.3
Sr	24.7	60.0	16.2	14.8	1.5	4.5
Y	24.1	3.9	9.7	12.0	2.1	294.7
Zr	52.1	25.9	40.3	16.2	11.4	5.4
Nb	7593.5	798.3	2276.8	302.2	17.6	1294.7
Mo	584.4	5.7	33.3	2.4	2.1	1047.1
Ag	0.0	0.0	0.0	107.3	16.7	8.7
Cd	0.0	0.0	0.0	0.0	0.0	0.2
In	161.1	0.7	7.3	2.5	0.3	1.1
Sn	194.5	13.2	12.9	16.6	9.9	8.1
Sb	5.2	4.7	3.1	4.5	5.2	23.8
Ba	96.9	1.8	150.8	10.5	0.2	0.7
La	5.0	0.2	1.8	5.1	0.8	0.1
Ce	32.7	0.5	4.9	9.7	0.6	0.6
Pr	4.1	0.0	0.5	1.0	0.0	0.0
Nd	13.5	0.1	3.3	3.6	0.1	0.8
Sm	5.5	0.0	0.8	0.8	0.0	2.5
Eu	0.0	0.0	0.2	0.9	0.0	0.0
Gd	4.7	0.3	1.2	1.0	0.1	10.3
Tb	1.3	0.1	0.6	0.2	0.0	4.9
Dy	11.4	1.2	8.7	2.1	0.2	60.5
Ho	2.8	0.4	2.5	0.5	0.1	18.8
Er	13.3	2.0	12.5	1.8	0.7	92.7
Tm	4.3	0.5	3.6	0.3	0.2	25.7
Yb	53.2	6.5	38.5	2.4	2.7	288.6
Lu	10.2	1.4	6.8	0.3	0.6	61.7
Hf	2.4	0.6	0.3	0.0	0.0	nd7
Ta	1403.5	595.7	747.7	778.5	616.2	652.5
Tl	0.0	0.0	0.0	0.0	0.0	0.0
Pb	1.2	0.4	0.0	0.4	0.0	0.3
Bi	0.0	0.0	0.0	0.0	0.0	96.4
Th	16.1	1.7	1.7	1.8	2.0	2.9
U	256.9	64.1	10.9	2.9	0.8	2.4

*Analyzed by Agilent ICP-OES using external standards

Table 3-21. Trace Elemental Composition Analyzed by Varian 820 ICP-MS using standard addition

Element(ppm)	USA2	USA3	UGA	ENG	BOH	USA4
Be	0.2	0.0	0.3	0.0	0.0	0.0
Na*	475.8	54.4	60.5	27.6	93.8	419.3
Mg*	426.8	328.7	128.2	158.1	3824.0	168.8
Al*	2555.7	2359.2	2860.7	1414.9	1731.5	1136.4
K*	641.8	0.0	987.4	0.0	41.4	35.0
Ca*	3406.7	747.2	816.5	1007.8	687.9	1182.4
Sc	2.9	9.2	0.2	5.3	37.2	686.6
Ti*	171.4	126.9	48.1	234.7	133.4	269.0
V	0.0	0.0	0.0	0.0	0.0	0.0
Cr	0.0	0.0	0.0	0.0	0.0	0.0
Co	1.2	1.0	76.3	0.6	7.6	0.2
Ni	7.9	10.3	64.1	9.8	13.6	5.9
Cu	36.7	4.2	6.8	9.0	6.9	4.5
Zn	277.9	76.1	349.9	105.4	65.8	144.3
Ga	23.1	5.6	0.0	10.1	4.3	20.3
Ge	15.2	5.2	0.8	7.6	4.0	14.2
As	29.4	40.9	93.5	30.2	2154.6	76.0
Rb	1.4	0.4	1.2	0.3	0.6	0.2
Sr	59.8	2.0	10.5	1.7	1.9	2.2
Y	31.6	39.2	65.3	5.5	37.1	9.6
Zr	32.2	10.5	6.6	13.5	8.7	85.6
Nb	2544.3	355.0	17.7	1418.4	710.0	5041.7
Mo	43.1	3.7	16.7	1.1	2.0	8.4
Ag	1.2	16.3	22.4	0.0	0.0	0.0
Cd	0.0	0.0	0.0	0.0	0.0	0.0
In	0.7	1.6	0.0	4.9	1.0	27.9
Sn	16.7	9.6	8.0	236.3	13.4	253.6
Sb	4.3	4.9	5.1	5.6	6.0	10.6
Ba	939.0	1.5	356.6	0.9	5.6	1.4
La	6.0	0.8	5.3	3.6	0.7	0.1
Ce	12.0	0.8	12.0	7.6	1.1	0.3
Pr	1.3	0.0	2.0	0.8	0.1	0.1
Nd	5.1	0.3	9.2	3.5	0.5	0.2
Sm	1.0	0.3	2.8	1.0	0.2	0.6
Eu	0.2	0.0	1.0	0.1	0.7	0.0
Gd	1.5	1.3	4.8	0.9	0.6	1.2
Tb	0.4	0.8	1.1	0.1	0.2	0.9
Dy	5.9	10.9	10.8	1.5	5.1	13.3
Ho	1.9	3.1	2.5	0.4	1.9	3.5
Er	9.5	16.1	9.9	2.4	10.4	18.8
Tm	2.4	5.1	1.8	0.7	2.9	6.3
Yb	27.3	63.5	14.4	9.9	31.0	72.6
Lu	6.0	12.8	2.3	2.1	6.3	13.2
Hf	0.6	0.0	0.0	0.1	0.0	7.2
Ta	968.7	652.7	689.6	713.3	706.1	1678.1
Tl	0.0	0.0	0.0	0.0	0.0	0.0
Pb	0.0	1.6	0.0	0.0	1.0	41.2
Bi	0.0	0.0	0.0	0.0	2.4	0.0
Th	3.5	2.3	3.5	2.4	2.9	3.4
U	34.0	0.9	1.6	2.7	1.5	53.8

*Analyzed by Agilent ICP-OES using external standards

Table 3-22. Trace Elemental Composition Analyzed by Varian 820 ICP-MS using standard addition

Element(ppm)	CR	PER	KOR
Be	0.0	0.0	0.0
Na*	107.8	160.0	48.7
Mg*	105.5	162.9	247.0
Al*	1331.7	1560.6	1765.0
K*	365.8	128.1	101.0
Ca*	3219.3	711.5	621.0
Sc	1632.3	119.2	25.3
Ti*	380.5	390.6	251.2
V	0.0	16.8	0.0
Cr	1.0	0.0	0.0
Co	0.5	0.6	2.4
Ni	6.9	18.9	6.5
Cu	12.7	1.9	5.5
Zn	236.7	24.3	133.4
Ga	15.7	19.0	12.5
Ge	10.7	11.2	7.8
As	104.5	27.6	28.0
Rb	3.8	0.4	1.0
Sr	7.6	1.8	0.6
Y	10.3	13.4	91.9
Zr	75.1	26.8	47.7
Nb	5854.9	60.7	3887.0
Mo	290.0	0.8	4.9
Ag	19.6	1.3	32.1
Cd	0.0	0.0	0.0
In	174.9	1.6	12.9
Sn	187.6	16.1	104.6
Sb	4.5	8.4	4.7
Ba	128.3	0.5	0.3
La	1.6	0.1	0.1
Ce	7.5	0.3	0.4
Pr	1.2	0.0	0.0
Nd	4.2	0.1	0.5
Sm	2.2	0.3	1.6
Eu	0.1	0.4	0.7
Gd	1.8	1.1	6.6
Tb	0.8	0.5	3.4
Dy	9.0	5.6	38.6
Ho	2.3	1.4	9.6
Er	12.8	5.7	39.4
Tm	4.6	1.2	9.5
Yb	58.7	10.2	89.5
Lu	10.9	1.7	14.7
Hf	7.1	0.2	1.2
Ta	1522.8	542.6	726.9
Tl	0.0	0.0	0.0
Pb	1.6	0.1	1.2
Bi	30.6	0.0	1.3
Th	15.7	3.5	1.7
U	89.6	39.8	44.6

* Analyzed by Agilent ICP-OES using external standards

Vegard's law states that the lattice parameters of a solid solution series containing two constituents are an equal mixture of those two constituents' respective lattice parameters if they crystallize under identical or equilibrium pressure, temperature and composition, also know as P-T-X conditions (Denton 1991). Deviations from Vegard's law are common in the case of metallic solutions, and even more common if the mineral in question is not cubic. Wolframite for example is monoclinic, and has a deviation from linearity due to temperature differentiation at the time of formation (Suryanarayana 1998). It is also possible that, if subjected to pressure, one element within the crystal structure may be more easily compressed (for example Fe or Mn) due to varying thermodynamic stability or elastic properties, which could help explain unequal mixing of the constituents in question within a solid solution series such as wolframite (Friedel 1954). Also the number and type of constituents in each of the sample's crystal lattices differ, as trace elemental compositions for each sample vary widely.

Wolframite is found in high temperature hydrothermal veins as well as moderate and low-temperature veins. Wolframite occurs in altered granitic rocks as well as metamorphic deposits adjacent to granitic intrusions (Hsu 1976). Elemental studies carried out in 1961 by Barabanov demonstrate that wolframite's composition varies widely not only within a given deposit, but also within an individual vein. He concluded that the identity of any particular wolframite sample is the result of local reactions with host rock. The composition of wolframite is not as much a reflection of the pressure and temperature conditions during formation or even the composition of the original solutions, as is it of the composition of surrounding rocks (Gundlach 1967).

Within this study, chemical analysis revealed that of the 15 samples, seven can be classified as hübnerites: SAX, USA1, USA2, USA4, CR, PER and KOR, and eight can be classified as ferberites: AUS1, POR, BOL, AUS2, USA3, UGA, ENG and BOH.

Trace elements consistently found in quantities near or above 1000 ppm appear to be Mg, Al, Sc, Nb, and Ta, as well as Ti and Zn to a lesser degree. In specific instances, other trace elements are also present in quantities exceeding 100 ppm; For example, Sn found in samples SAX, ENG, and USA4, as well as CR. Uranium concentrations in sample SAX were found to be 256.9 ppm, whereas no other sample has U concentrations exceeding 90 ppm. Samples SAX and CR have Sc concentrations in excess of 1600 ppm, at least more than double any other sample. Samples BOL UGA and PER have low amounts of Nb: <100 ppm, whereas each of the other 13 samples have Nb concentrations >300 ppm with most Nb values exceeding 1000 pm. SAX, USA4 and CR have more than double the amount of Ta than any other samples at concentrations exceeding 1400 ppm.

Overall, hübnerites have at least three times more Zr than ferberites. Sample AUS1 has more than double the amount of K found in any other sample at 2120.5 ppm. Sample AUS2 was found to have 96.3 ppm Bi, whereas each of the other 14 samples either contain no detectible amounts of Bi or have Bi concentrations at least 60 ppm less than sample AUS2. Sample AUS2 also has Y concentrations of 294.7 ppm whereas no other sample has more than 90 ppm Y. Sample AUS2 has 5 times the amount of any other sample in terms of Yb content at 288.6 ppm. A similar relationship can be found in sample BOL in that Au concentrations were found to be >100 ppm, whereas no other sample comes close in terms of ppm Au. Sample UGA is the only sample with more than 10 ppm of Co, containing 76.2 ppm Co, while most samples are <1 ppm Co.

3.3. P-XRD

Largest P-XRD peaks including reflection intensity are given in Tables 3-23. and 3-24.

3-23. Largest P-XRD Peaks Including Reflection Intensity

	(130)		(030)		(020)		(11-1)	
Sample	d	I/I_{100}	d	I/I_{100}	d	I/I_{100}	d	I/I_{100}
SAX	1.7775(2)	34.91	1.9146(9)	3.80	2.8729(5)	5.58	2.9788(4)	20.64
USA1	1.7831(2)	41.81	1.9205(2)	15.76	2.8789(3)	26.77	2.9942(6)	20.34
AUS1	1.7677(8)	63.78	1.9043(6)	100.00	2.8554(5)	100.00	2.9369(3)	100.00
POR	1.7688(3)	33.99	1.9066(4)	8.63	2.8625(4)	14.96	2.9400(4)	47.58
BOL	1.7672(2)	23.77	1.9029(10)	1.41	2.8542(7)	3.63	2.9368(5)	22.89
AUS2	1.7716(3)	30.24	1.9094(6)	3.15	2.8670(5)	4.71	2.9508(4)	31.93
USA2	1.7828(2)	53.48	1.9185(3)	7.08	2.8779(7)	12.21	2.9912(4)	19.62
USA3	1.7683(3)	32.26	1.9063(3)	9.54	2.8600(3)	13.91	2.9412(5)	44.58
UGA	1.7625(4)	16.94	1.8995(4)	2.98	2.8498(5)	3.85	2.9306(3)	53.06
ENG	1.7748(4)	29.61	1.9129(2)	28.07	2.8701(2)	42.61	2.9664(3)	13.98
BOH	1.7677(2)	31.91	1.9053(2)	6.16	2.8551(5)	6.45	2.9401(3)	42.95
USA4	1.7800(2)	46.30	1.9329(3)	10.69	2.8780(1)	2.42	2.9844(8)	10.28
CR	1.7775(8)	100.00	1.9133(2)	26.30	2.8717(3)	19.79	2.9744(7)	18.03
PER	1.7843(3)	38.13	1.9207(2)	9.35	2.8843(4)	14.53	2.9956(4)	31.19
KOR	1.7797(2)	36.26	1.9162(4)	5.97	2.8761(4)	7.26	2.9509(3)	45.81
High=	*1.7843(3)*	*100.00*	*1.9329(3)*	*100.00*	*2.8843(4)*	*100.00*	*2.9956(4)*	*100.00*
Low=	*1.7625(4)*	*16.94*	*1.8995(4)*	*1.41*	*2.8498(5)*	*2.42*	*2.9306(3)*	*10.28*

3-24. Largest P-RXD Peaks Including Reflection Intensity (cont'd)

	(110)		(011)		(100)		(010)	
Sample	d	I/I_{100}	d	I/I_{100}	d	I/I_{100}	d	I/I_{100}
SAX	3.6821(5)	70.29	3.7709(9)	59.24	4.7968(4)	28.06	5.748(3)	4.87
USA1	3.6950(6)	80.65	3.7729(7)	72.66	4.8220(7)	42.86	5.7598(10)	39.12
AUS1	3.6490(8)	100.00	3.7455(2)	50.56	4.7369(1)	100.00	5.7000(10)	100.00
POR	3.6583(7)	57.80	3.7566(6)	61.36	4.7522(2)	31.75	5.7223(9)	18.24
BOL	3.6459(2)	36.37	3.7436(9)	51.37	4.7368(5)	23.72	5.708(3)	4.57
AUS2	3.6654(10)	45.47	3.7567(10)	54.68	4.7734(10)	31.33	5.735(3)	4.95
USA2	3.6923(8)	77.42	3.7774(1)	52.18	4.825(2)	25.10	5.7542(6)	24.54
USA3	3.6625(5)	45.68	3.7568(4)	78.28	4.7548(3)	32.10	5.709(2)	13.30
UGA	3.6334(8)	58.38	3.7402(8)	69.04	4.7159(2)	47.96	5.702(3)	5.86
ENG	3.6771(9)	50.62	3.7687(8)	46.38	4.8010(4)	25.52	5.7414(1)	52.78
BOH	3.6486(2)	32.78	3.7493(3)	37.39	4.7416(6)	18.01	5.719(3)	8.04
USA4	3.6937(9)	27.47	3.7732(8)	44.07	4.7932(9)	16.82	5.776(4)	2.97
CR	3.6789(9)	62.38	3.7696(9)	61.17	4.7822(8)	51.08	5.7404(5)	14.50
PER	3.7040(7)	58.01	3.7754(6)	100.00	4.8328(3)	37.11	5.7652(6)	21.80
KOR	3.6833(7)	51.82	3.7690(7)	64.48	4.8058(4)	29.15	5.750(3)	9.67
High=	*3.7040(7)*	*100.00*	*3.7774(1)*	*100.00*	*4.8328(3)*	*100.00*	*5.7760(4)*	*100.00*
Low=	*3.6334(8)*	*27.47*	*3.7402(8)*	*37.39*	*4.7159(2)*	*16.82*	*5.7000(10)*	*2.97*

In looking at the eight largest powder x-ray diffraction peaks, *d* values for hübnerites are consistently larger than ferberite d values. One exception is sample ENG, which although it has chemically been determined to be a ferberite, has *d* values more akin to the hübnerites. This relationship can be explained by looking at the metallic radii of the elements Fe and Mn. Mn has an ionic radii of 1.30 Å, whereas Fe has a ionic radii of 1.26 Å. Because ferberites contain more Fe, its *d* value is also smaller as a result for each of the eight reflections considered. Intensity appears to be random in the sense that hübnerites do not yield more intense reflections than ferberites for example, or vice versa.

3.4 Raman

No conclusive data were gathered using Raman Spectroscopy; Figure 3-9 shows wolframite spectra in terms of Raman shift 1/cm.

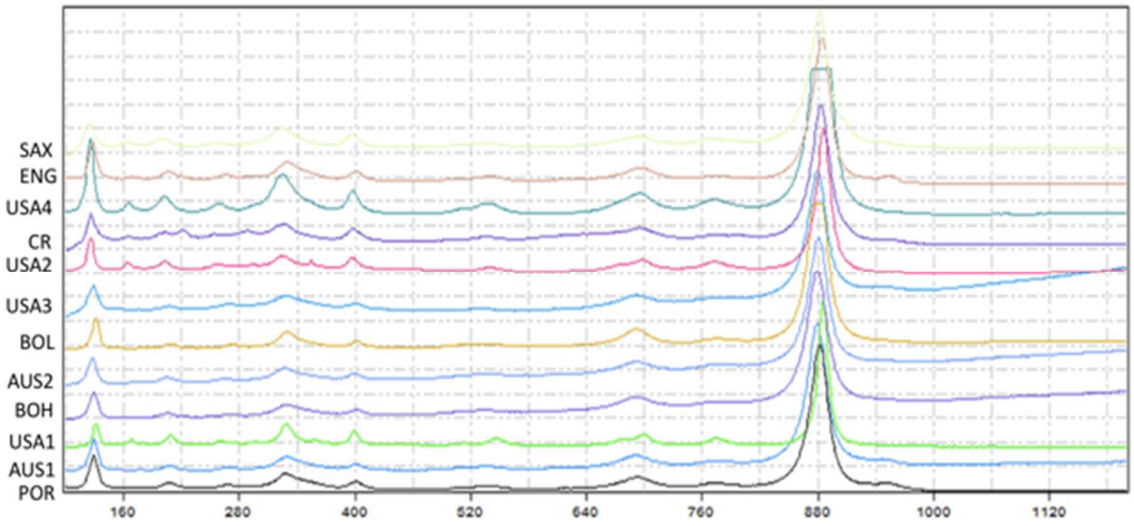

Figure 3-9. Raman Spectra showing Raman Shift (cm^{-1})

3.5. Statistics

Ward's method of hierarchical clustering was used to determine if SC-XRD, P-XRD, ICM-PS, ICP-OES and Raman data would cluster based primarily on separating those samples that tended to have higher values over all from those which had lower values over all. Clustering analysis is sometimes effective in distinguishing hübnerites from ferberites, but not always. Figures 3-9 through 3-15 show how some data sets are more valuable for these purposes than others.

On the dendrograms below each color represents a group that a sample is categorized into based on likenesses to other samples. Figure 3-15 takes into account all the data collected and sorts the samples into two groups, pink and green. We know that the samples within the pink section are hübnerites and the samples within the green section are ferberites. Other colors represent samples that do not fit into a group due to a lack of shared characteristics.

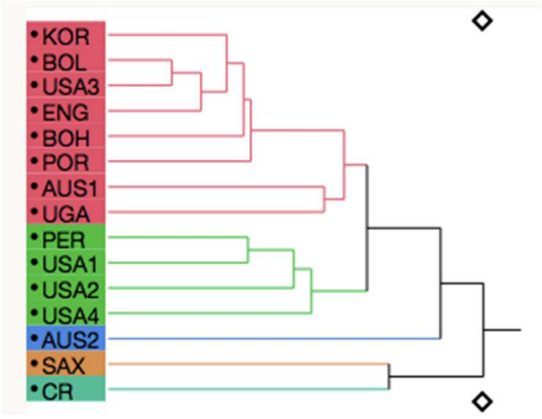

Figure 3-10. All Chemical Data Cluster Analysis Dendrogram

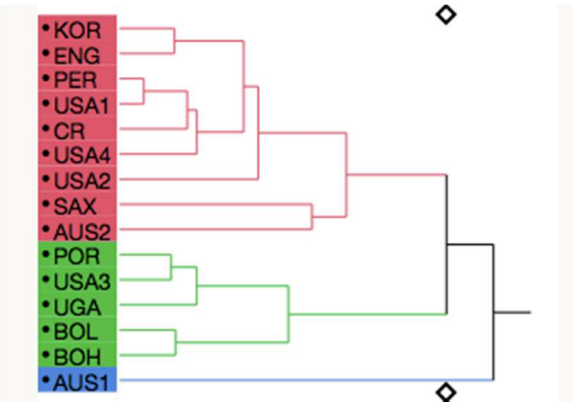

Figure 3-11. Major Elemental Data Cluster Analysis Dendrogram

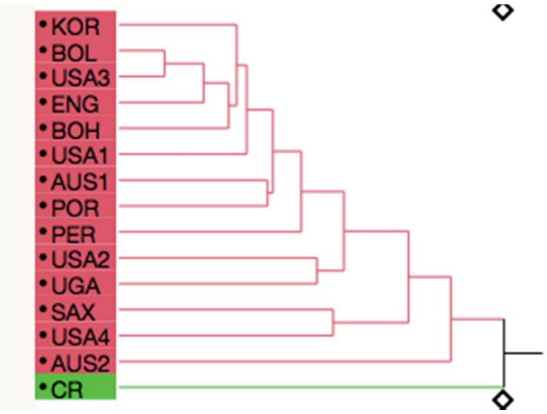

Figure 3-12 Trace Elemental Data Cluster Analysis Dendrogram

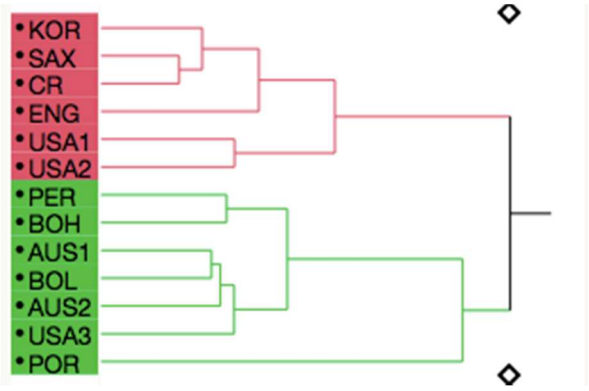

Figure 3-13. SC-XRD Data Cluster Analysis Dendrogram

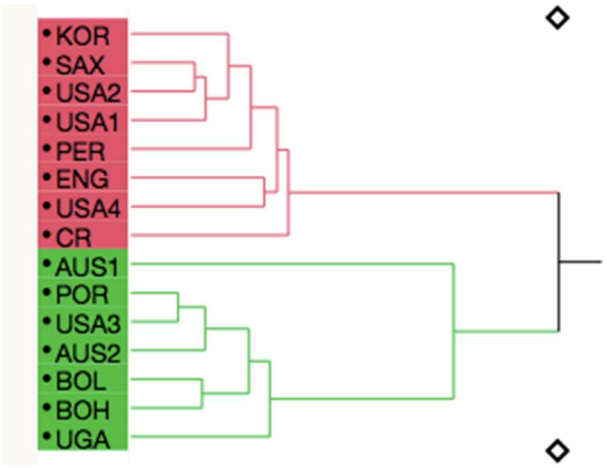

Figure 3-14. P-XRD Data Cluster Analysis Dendrogram

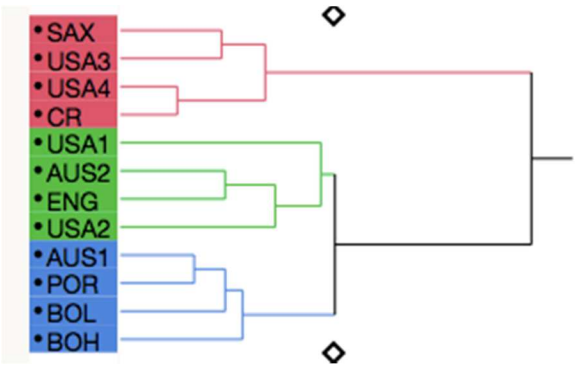

Figure 3-15. Raman Cluster Analysis Dendrogram

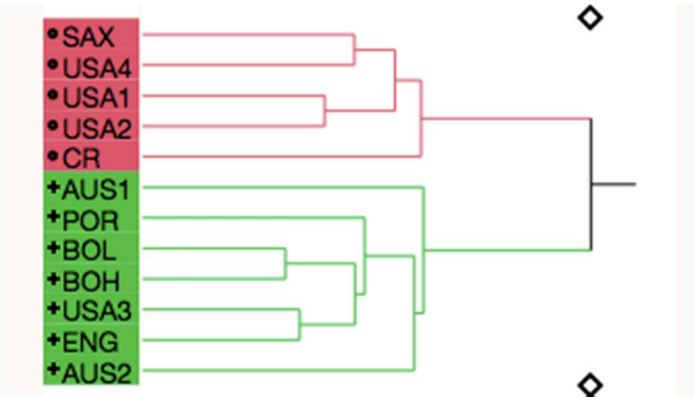

Figure 3-16. All Data Cluster Analysis Dendrogram

Performing clustering analysis on all of the chemical data, both major and trace elemental compositions (when considered together) did not yield a perfect split of hübnerites and ferberites. A few samples are sorted into their own groups rather than being clustered with the other hübnerites or ferberites respectively, making these data set less effective in finding similarities in like samples that could help categorize an unknown sample based on criteria akin to that of a known group (3-9).

When major elemental data was used to create clusters, hübnerites and ferberites were distinguished from one another as separate, distinct groups (3-10). Trace elemental data were so unique and varied widely for each sample, which might ultimately make for the best fingerprint, and was ineffective in clustering at all (3-11). It would be interesting to see if the data for each sample would cluster with other samples taken from the same mine sites, thus establishing a unique chemical fingerprint for a specific locality. SC-XRD data were only slightly more informative than the major elemental data analysis (3-12). P-XRD data on its own were by far the most effective in terms of clustering samples into two distinct groups that are ferberites and hübnerites respectively (3-13). Raman data was not very informative, with a scattering of clusters much like those found in the "all chemical data" dendrogram (3-14). The only data set that allowed for perfect clustering/separation of hübnerites and ferberites with no misplaced samples was the entire data set as a whole, including all of the ICP-MS, ICP-OES, SC-XRD, P-XRD and Raman data (see figure 3-15).

Linear, common covariance discriminate analysis was used to determine if it was possible to predict something about a sample based on SC-XRD, P-XRD, ICM-PS, ICP-OES and Raman data, respectively. For example, with all of the data available, how

accurately it is possible to predict what geologic environment an unknown sample is from using an algorithm generated in terms of a linear common covariance discriminate analysis in order to (from what may appear at first to be random or unrelated data sets) create identities, or at least identify regional similarities?

Another concern for this study was the generation of a usable function *via* linear common covariance analysis in JMP. Although there was not a predetermined amount of data that was known to be "enough" data to be able to effectively characterize data and put it into a proper category going into this study, we found that the amount of data available at this time (generated both within and outside of the scope of this study) on the wolframite family of minerals was insufficient. This led to the attempted classification of too few rows of data into too many groups, which resulted in the generation of functions that are not usable. In order to classify 21 samples of data into five groups, a minimum of four functions were needed. Because the four functions that were generated didn't classify our known samples well, we certainly could not apply them to unknown samples and expect accurate classification. A function or functions that could predict which group our samples would fall into with high probability could not be created at this time, but with more data it is possible that the appropriate function or functions could be created.

CHAPTER 4: DISCUSSION

Future mineral fingerprinting studies might explore other analytical techniques, such as X-ray fluorescence (XRF) in an attempt to determine chemical variability within one deposit, as opposed to comparing 15 wolframite samples from 15 different localities all over the world. For example, selecting multiple samples from a single ore body would define intra-deposit variability in terms of chemistry and crystal structure, which is unknown as of now. Moving forward, mineral fingerprinting on the local scale (versus global) could be a more realistic aim for minerals with sufficient crystallographic and chemical variability.

Focusing more on one region's specific geological situation/history might help in understanding *why* wolframite from one deposit differs from another, nearby deposit, (or not) going a step further than this study, which has instead looked more at *if* there was variability along the wolframite solid solution series, and *how much?* Now that we have a better understanding of wolframite, we can say with certainty that there is variability and the amount of that variability is extensive. If a large enough database existed that catalogued those unique and potentially subtle differences in wolframites from place to place, which could be used as a reference when looking at the atomic structures and chemistry of samples in question, samples in hand could be compared with those on the database.

Would it then be possible to pick up a piece of wolframite (raw ore/unsmelted material) and determine, based on its mineralogy after testing, where it is most likely to have been mined from? How specific it is possible to get is significant, because if this method only allows us to determine with relative certainty a general area versus a

particular ore body the mineral derives from, that could be the difference between an illegal mining operation and a legal one next door, and would thus not be specific enough to be helpful in a political sense.

Even in a scenario where a detailed enough database existed, if supply chain paperwork documents that a mineral is from a place other than what testing suggests, what can be done? More legal complications and questions about regulatory policies arise. In light of a rapid and ever-changing political climate, the status of the Dodd Frank Act going forward may change. Social and political conflicts in the DRC, both historical and current, although linked to wolframite, have very little to do with the science of mineralogy and are discussed minimally in this paper, but cannot be ignored when discussing wolframite and the role in plays in society. When studied in this context, it should be emphasized that there is still much to learn about the wolframite solid solution series and how its management affects various cultures and peoples.

It would also be beneficial in the pursuit of better understanding the wolframite family of minerals to learn more about the polycrystalline variety reinite. Along the tungsten belt in central Rwanda, tungsten mineralization is hosted by quartz veins and is often present in the particular form of reinite, which represents a polycrystalline pseudomorph of ferberite after scheelite. There is still debate on the genesis of these tungsten deposits, though the tungsten deposits of Rwanda and Uganda have been interpreted to be epigenetic in origin (Frisch 1975).

The occurrence of reinite is only reported from a few localities worldwide, for example, from the Cu-W-bearing tourmaline breccia pipe of Ilkwang (Korea), Kimbosan and Sannotake deposits (Japan), Mount Misobo (DRC), Rutsiro area (Rwanda) and

several tungsten deposits in the Kigezi district in southwest Uganda, which show very similar geological characteristics to the Rwandan deposits. These directly abut the North and South Kivu provinces of the DRC, where conflict minerals are mined (Goldmann et al. 2013).

The Central African Tungsten Province contains numerous tungsten deposits wherein the Fe-rich members of the wolframite family are responsible for the region's sole economic tungsten source. Two variations of the solid solution series have been documented in this locality. Some ferberite can be found as black crystals with uniform orientation and large, reflective cleavage planes. These crystals are primarily unaltered. Found alongside these ferberite crystals are fine-grained clusters of a dark colored, dull material with no visible cleavage planes. It is thought that these two ferberite varieties record two distinct generations, the latter of which is reinite (Sahama 1981).

In this study, sample UGA is geographically closest to the conflict mining regions in the DRC, and although a single grain could not be extracted for single crystal diffraction as it was found to be polycrystalline reinite, this in itself is a noteworthy, as reinite occurrences are not common, as mentioned above. Though it was not possible to gather atomic data from this sample, that simple fact in and of itself helps to narrow down possible places of origin for this and potentially other reinite samples in question, as the list of known localities in which this mineral can be found is short.

CHAPTER 5: CONCLUSIONS

There are four conflict minerals identified by the USGS and the US Securities and Exchange Commission (SEC), and in accordance with the Dodd Frank Act Section 1502, corporations using those conflict minerals in manufacturing processes must demonstrate that they are sourced ethically, i.e., not from conflicted areas or in illegal ways, as has been the case in some parts of the Democratic Republic of Congo. There are two ways to verify the provenance of mineral samples: chain of custody, and a fingerprinting method for conflict minerals.

In this study we examined the conflict mineral wolframite as a proxy. We found that the range of crystallographic, chemical and other spectroscopic properties of wolframite was unknown. Therefore, the first step in this study was to collect a suite of 15 members of the hübnerite-ferberite solid solution series and determine the range of various values in those minerals. To do that we collected single crystal X-ray diffraction data, powder X-ray diffraction data, Raman spectroscopy data, inductively coupled plasma mass spectrometry data as well as inductively coupled plasma optical emission spectrometry data.

We then used statistical methods to determine relationships between samples. The results of that work shown above confirm that there is no firm method at the present time of determining the provenance of a sample based on the information of the crystal structure, diffraction patterns, vibrational frequencies/scattering, or major and trace elemental chemistry. We did find that we can identify clusters based on major element cation composition, i.e., Fe *vs*. Mn, (ferberite *vs*. hübnerite).

In 2014, part of section 1502 within Dodd Frank was struck down by a U.S. appeals court when the U.S. National Association of Manufacturers and the Chamber of Commerce sued the SEC, saying that the law took away their freedom of speech in forcing companies to state whether or not their products contained conflict minerals. Other aspects of the conflict minerals rule were untouched, requiring companies to continue reporting the details of any findings pertaining to conflict minerals in their supply chain to the SEC. These findings are then publicly filed, maintaining the transparency and due diligence required by law in adherence with the Act (Lynch and Stephenson 2017).

Some of the civil societies that disagree with this ruling have presented the irony of the attack on Dodd-Frank coming from US companies it was intended to help. The entities affected most by this ruling: mining communities throughout DRC and surrounding areas initially saw the Dodd-Frank Act as another regulatory imposition pushed upon them without consultation of their own local Government. Over time communities within this region have come to embrace the challenges that have come with this new policy initiative and agree that the effects of this new policy are having a real tangible positive effect in the DRC and beyond (PACT 2015).

What is left of section 1502 within the Dodd Frank is now under fire by the current administration. A policy advisor with nonprofit group Global Witness for human rights, Carly Oboth, said in a public statement on Wednesday February 8, 2017: "This law helps stop U.S. companies funding conflict and human rights abuses in the Democratic Republic of Congo and surrounding countries. Suspending it will benefit secretive and corrupt business practices. Responsible business practices are starting to

spread in eastern Congo." Progress made could be undone with the removal of laws protecting people's safety and wellbeing.

As explicitly stated within the Dodd Frank Act, the president of the United States can suspend or change mandates within the Act for up to two years if the safety and security of the country is at risk. Were the SEC to perform such a suspension at the request of President Trump it would be in response to several businesses that have opposed the law, saying it imposes expensive regulations that are difficult to uphold, ultimately forcing American companies to lose money and cut American jobs, putting undo stress on productivity and the economic growth of the US. If mining companies have an incentive to stop using minerals from a particular region, mining communities where legal mining is occurring nearby may also be hurt by Dodd Frank.

In early 2017, using the Congressional Review Act (CRA), the House GOP voted to kill another section of Dodd Frank requiring oil, gas, and mining companies to disclose payments made to foreign governments. The CRA allows the House and Senate to repeal regulations finalized after June 13, 2016 by a simple majority vote with the support of the President. The House has voted to kill the "resource extraction rule", and as of March 2017 the Senate has yet to vote. If when they do vote the rule is overturned, under the CRA, the SEC can not craft a new rule that is "substantially the same form" as the piece of repealed regulation, but Dodd-Frank still requires the SEC to provide a transparency rule. (Plumer 2017).

Although it is known that the underlying root cause of the fighting and civil unrest that took place in central Africa from 1997 to 2003, known as Africa's World War, is only partially linked to the region's natural resource wealth (Global Witness 2015), it is

clear that illegal forces in the sectors of mining as well as taxation and transport of minerals in the DRC provided significant funding for the continuation of the violence. When derived from war torn areas in the DRC and nearby regions, wolframite is one of the four conflict minerals discussed above. Although prized as an economically significant source of tungsten ore, surprisingly little structural (atomic/crystallographic) data were available for wolframite prior to this study, and this this detailed exploration of the mineral wolframite will help to fill a knowledge gap in both the mineralogical realm as well as politically. Is it possible to trace wolframite back to its provenance for the sake of compliance with regulatory impositions and consumer demand? Not yet, but we are getting closer.

The Democratic Republic of Congo's (DRC's) vast mineral wealth has instigated instability, conflict, and corruption (Brydges 2013). The paradox of plenty theory, discussed by Richard Auty in his 1993 book Sustaining Development in Mineral Economies, The Resource Curse Thesis, can be applied to the DRC in that profits from mining fund violence, rather than improve people's lives (Reno, 2006). The DRC has a long and complex history of internal warfare financed by foreign actors (Carayannis 2003).

Humanitarian groups such as The Enough Project and Global Witness have also responded by to the crisis in the DRC by generating initiatives to raise awareness about the issues surrounding conflict minerals, encouraging people to ask more questions, and demanding conflict free products. The Enough Project's Raise Hope for Congo Campaign has developed a rating system for big technology companies based on how conflict conscious they are. These minerals are a particular source of conflict

because they are so economically valuable. Gold is an international is an standard of values, cassiterite is prized for tin, colton/columbite is used for niobium and tantalum, and wolframite is valued for tungsten. These elements are heavily relied upon for their many industrial uses.

The role that the rest of the world plays in war going on in the DRC is substantial. The sale of tin, tungsten, tantalum and gold has financed wars in the DRC for over a century, at the demand of industrialized nations. To prevent companies from inadvertently funding wars through the purchase of conflict minerals by offering a way to comply with the Dodd Frank Act, the intent of this project was to determine the chemical, structural and spectroscopic variability of samples from 15 localities worldwide, and to assess whether this variability will provide a method of fingerprinting valuable materials in response to rising and urgent demand. In building a knowledge base for this challenging subject, this project promotes accountability from the mine to consumers in the context of the mineral wolframite.

REFERENCES CITED

Autesserre, S. (2012). Dangerous Tales: Dominant Narratives on the Congo and their Unintended Consequences**.** *Oxford Journal of Social Sciences, African Affairs*.vol 111, no 443.

Auty, R. M. (1993). Sustaining Development in Mineral Economies: The Resource Curse Thesis. London: Routledge.

Barabanov, V. F. (1961). Mineralogy of East Transbaikalian Lltolframite Deposits. Vol. 1, Leningrad University Press.

Bloss, D. (1994). Crystallography and Crystal Chemistry. Mineralogical Society of America. 210.

Brydges, (2013). Colton. "Resource Conflict in the Democratic Republic of Congo." Carleton Review of International Affairs 2: 12-20.

Burns, R. (1970). Mineral applications of crystal field theory. Cambridge University Press. 7-32.

Burt, R. (2016). Much ado about Tantalum. Again. Published by MSA PIG Group, 2016http://www.minsocam.org/msa/Special/Pig/PIG_Articles/PIG_articles.html

Carayannis, T. (2013). The Complex Wars of the Congo: Towards a New Analytic Approach, Journal of Asian and African Studies, vol. 38, no. 2-3: 232-550.

Chasan, E. (2015). House Subcommittee Testimony Calls Conflict Minerals Rule a Failure. The Wall Street Journal. Published online Nov 17th.

Cuvelier, J. ET AL (2014). Analyzing the Impact of the Dodd-Frank Act on Congolese Livelihoods. Conflict Prevention and Peace Forum. Published online by the Social Science Research Council.

Dachs, V.H., Stroll, E. & Weitzel, H. (1967). Kristallstruktur und magnetische Ordnung des Hubnerits, MnWO4. Zeitschrift fur Kristallographie. vol 125.

Denton, A., Ashcroft, N. (1991). "Vegard's law". Phys. Rev. A. 43 (6): 3161–3164.Electronic Industry Citizenship Coalition EICC. (2011) www.eicc.info/

Escobar, C., Cid-Dresdner, H., Kittle, P. & Dumler, I. (1971). The Relation Between "Light Wolframite" and Common Wolframite. The American Mineralogist. vol 56.

Friedel, J. (1955). “Deviations from Vegard's law”. The London, Edinburgh, and Dublin Philosophical Magazine and Journal of Science Series 7, Volume 46, Issue 376: 514-516.

Frisch, W. (1975). Die Wolfram-Lagerstiitte Gifurwe (Rwanda) und die Genese der zentralafrikanischen Reinit-Lagerstiitten. Jahrbuch der Geologischen Bundesanstalt, Wien, 118, 119-191.

Gbaruko, B. C., & Igwe, J. C. (2007). Tungsten: Occurrence, Chemistry, Environmental and Health Exposure Issues. *Global Journal of Environmental Research*, 1.1: 27-32.

Gianopoulos, K. (2015). Insights from Companies’ Initial Disclosures and State and USAID Actions in the Democratic Republic of the Congo Region. United States Government Accountability Office. Testimony before the Subcommittee on Monetary Policy and Trade, Committee on Financial Services, House of Representatives. SEC Conflict Minerals Rule. GAO-16-200T.

Global Witness. (2015). Conflict Minerals in Eastern Congo. https://www.globalwitness.org/campaigns/conflict-minerals/conflict-minerals-easterncongo/

Goldman, S., Melcher, F., Gäbler, HE., Dewaele, S., Clercq, F., & Muchez, P. (2013). Mineralogy and Trace Element Chemistry of Ferberite/Reinite from Tungsten Deposits in Central Rwanda. *Minerals* 3.2, 121.

Gundlach, H. (1967). Transport und Abscheidungsbedingungen von Wolframerzen aus Wasserigenlosungen. In, Pegmatische Lagerstatten und Ihre Wirtschaftliche Bedeutung. H. 19, Claus-thal-Zellerfeld.

Harker, R., et al. (2012). Geographical analysis of conflict minerals utilizing laser-induced breakdown spectroscopy.” *Spectrochimica Acta Part B: Atomic Spectroscopy,* vol. 74-75: 131-136.

Hsu, L.C. (1976). The Stability Relations of the Wolframite Series. Nevada Bureau of Mines and Geology, and Department of Geology and Geography Mackay School of Mines, University of Nevada, Reno, Nevada 89507American Mineralogist, Volume 61: 944-955.

ITRI. (2015b). https://www.itri.co.uk/index.php?option=com_mtree&task=viewlink&link_id=55397&Itemid=11

Kester, J. & Murphy, M. (2014). Companies Detail Use of ‘Conflict’ Metals- First Reports Filed to SEC on Potential Use of Minerals from a Region of War-Torn Africa. Wall Street Journal, online June 2nd.

Lezhnev, S. (2015). Over 140 Mines in Congo are Now Officially Conflict-Free: the Latest List. http://www.enoughproject.org/blogs/over-140-mines-congo-are-now-officially-conflictfree-latest-list, online October 2015.

Lynch, S. & Stephenson, E. (2017). White House plans directive targeting 'conflict minerals' rule: sources. Reuters News Agency. Commodities online article, February 8th.

Little, M. (2010). Conflict Minerals; GSA-USGS Congressional Science. Fellow Report, GSA Today, vol. 20, no. 11, 22.

Macavei, J. & Schulz, H. (1993). The Crystal Structure of Wolframite Type Tungstates at High Pressure. Zeitschrift fur Kristallographie. vol 207.

Mcmanis, C. (2015). Determination of Diamond Provenance is Possible with Multivariate Analysis of LIBS Spectra. 2015 GSA Annual Meeting in Baltimore, Maryland, USA (1-4 November 2015) Paper No. 300-4.

Melcher, F., et al., (2008). Fingerprinting of conflict minerals: columbite-tantalite ("coltan") ores. *SGA News,* no. 23.

OECD. (2011). OECD Due Diligence Guidance for Responsible Supply Chains of Minerals from Conflict-Affected and High-Risk Areas, OECD Publishing. http://dx.doi.org/10.1787/9789264111110-en

Oliviera, E.C. ET AL (2010). Internal standard versus external standard calibration: an uncertainty case study of a liquid chromatography analysis. Química Nova, vol.33 no.4 São Paulo: 1.

PACT. (2015). Unconflicted – Making conflict-free mining a reality in the DRC, Rwanda and Burundi. http://www.pactworld.org/sites/default/files/unconflicted.pdf

Plumer, B. (2017). On the same day Rex Tillerson is confirmed, the House votes to kill a transparency rule for oil companies. http://www.vox.com/2017/2/1/14477314/oil-companies-disclosure-rule-tillerson

Sahama, G. (1981). The Secondary Tungsten Minerals, A Review. The Mineralogical Record. March-April, 81.

Sheldrick, G. (2008). A Short History of SHELX. Acta Cryst. 64, 112-122.

Shedd, K. (2000). "Tungsten" *USGS Mineral Resource Program: Commodities*.

Smith, E. & Dent, G. (2005): Modern Raman Spectroscopy: A Practical Approach. J. Wiley Hoboken, NJ.

Suryanarayana, C. & Norton, M. (1998): X-Ray Diffraction, A Practical Approach. Springer Science+Business Media LLC. 178.

Reno, W., (2006). "From State Collapse to 'Absolutism' to State Failure," Third World Quarterly, vol. 27, no. 1: 43-56.

Ulku, V.D. (1967). Untersuchungen zur Kristallstruktur und magnetischen Stuktur des Ferberites FeWO4. Zeitschrift fur Kristallographie. vol 124.

US Securities and Exchange Commission H.R. 4173 — 111th Congress (2009). Dodd-Frank Wall Street Reform and Consumer Protection Act." www.GovTrack.us.

Willhite, J. (2014). 'Conflict' Metals Disclosures Roll Out. The Morning Ledger, online June 3rd.

APPENDIX

Samples from this study were procured from the Harvard Mineralogical Museum (HMM). These samples were donated from various sources and with varying degrees of detail included. The HMM passed along all of the available background information for each sample, though very little was definitively known. For some samples the name of the city or general region that it is thought to have potentially came from is known, whereas with other samples only the state or country of origin was known. This being the case it is difficult to find a definitive starting point for research into ages of the deposits that each of these minerals hails from, respectively. Using the descriptions/terminology that was provided with each sample, and www.mindat.org as a resource, some generalized information is summarized below based on the approximate locations given, which in some cases were found to be unofficial or undocumented names for mines or mining areas.

Sample KOR was purchased for this study, and procured from the Tae Hwa Mine in Chung Cheung Buck Oo, Korea. The geology of this region is a quartz-vein type tungsten deposit. The mine opened in 1902, and was abandoned in 1973. Dumps were reclaimed in 2000, and are now mostly revegetated. About twenty-two minerals are documented for this site, including ferberite, wolframite, scheelite, and cassiterite.

Sample PER was was purchased for this study, and procured from the Mundo Nuevo Mine in Mundo Nuevo, Huamachuco Sanchez Carrion Providence, La Libertad Department, Peru. This mining area is high in the Andes range. Tungsten ore is found in quartz veins. Twenty-two minerals are documented for this locality including hübnerite, hydrotungstite, and scheelite.

Wolframite sample SAX (as well as the rest of the minerals I discuss were procured from the Harvard Mineralogical Museum) comes from a famous tin deposit, half of which is in Saxony Germany (Zinnwald) and half of which is in Bohemia, Czech Republic. A stockwork of quartz, cassiterite and wolframite veins are found within greissens along the contact of a granitoid cupola intrusion. About ninety minerals are found in this location including hübnerite, ferberite, wolframite, scheelite, cassiterite and tungstate.

Wolframite sample USA1 is from Arizona but no other mine information/locality data is known/was given. Hundreds of documented cases of wolframite can be found in Arizona on Mindat.org.

Wolframite sample AUS1 is from the Torrington Mine in New South Wales (Clive Co.), Australia. There are upwards of a hundred documented wolframite localities in the Torrington region of Clive CO in South Whales. About fifty minerals are documented for this site including cassiterite, cobalt, hübnerite, ferberite, wolframite, gold and scheelite.

Wolframite sample POR is from Borralha, Portugal. Borralha mine was a producer of tungsten from 1903-1985, closing due to a decline in tungsten prices. Most of the tungsten coming from this region is in the form of wolframite, very little from scheelite. This area covers 127.5km of underground and open pit mines. Ore was mined primarily from vertical and subhorizontal veins along contact of granitic intrusions and sedimentary bedrock. Currently, breccia trenches are being excavated. Three distinctive mineralization episodes are known. Over thirty minerals have been documented for this site including scheelite, wolframite and tungstite.

Wolframite sample BOL is from Bolivia. There was no specific mine information/locality available. There are hundreds of documented cases of Wolframite found in Bolivia (Mindat.org). Bolivia's production of tungsten slowed in the 1980s (just as was the case in Portugal) due to a decline in tungsten prices. Currently Bolivia is still one of the top ten tungsten producers in the world according to the USGS.

Based on the information we were given, wolframite sample AUS2 is either from the Wolframite Camp in Northern Queensland, Australia or the Wolfram Camp, Dimbulah, Mareeba Shire, Tablelands Region (Near Cairns). Branching pipe-like quartz-rich molybdenite-wolframite-bismuth pipes occur within the altered margin and roof zone of a course grained granitic pluton. The mine may have opened as early as 1894. Fifteen minerals are documented for this site including wolframite, ferberite, scheelite and molybdenite.

Wolframite sample USA2 is from Williams Mine in Big Sandy, Arizona. Mohave Co. (far NW part of Arizona). The mine opened in 1902 known as Tungsten Mines Co. between 1915-1917 and was then owned by the Continental Mining Corp in 1940. Coarse grained glassy gray quartz vein 1-2 feet wide are the host for wolframite found within a tabular ore body. Nine minerals are documented for this site including hübnerite, apatite, wolframite, scheelite and pyrite.

Wolframite sample USA3 is from Germania Mine in Stevens County Washington, USA. More specifically, Roselle Mine, Adams Mountain, Deer Tail and Cedar Canyon Districts, Huckleberry Range. This tungsten mine produced ore from 1904-1955 which was sent to Germany. The geology of this region is Jurassic and Tertiary age granite.

Wolframite sample UGA is from the Kirwa Wolfram Mine in Kabale, Uganda. As of 2012, this mine has been officially closed (a temporary mining ban is in place) by the state minister of minerals due to "improper procedures". There are no samples from this site documented on Mindat.org. One nearby mine site (Bjordal/Nyamuliro) that is found on Mindat is a documented locale for ferberite.

Wolframite sample ENG is from Cornwall, England. No specific mine information/locality available. According to Mindat, there are hundreds of mines on Cornwall England that have documented cases of wolframite. The generally geology of Cornwall ranges from granite, schist, sandstone to shale. As of 2007, there are no active metalliferous mines remaining.

Wolframite sample BOH is from Schlaggenwald, Bohemia. More specifically "Horni Slavkov" Karlvoy Vary Region, Czech Republic. Last mining activity here was in 1991. One hundred and sixty six minerals are documented for this site including wolframite, hübnerite, ferberite, scheelite and cassiterite.

Wolframite sample USA4 is from US Tin Corp in Lost River, Alaska. Seaward Penninsula, Port Clarence District, Nome Borrough. Greenstone lode deposits, underground skarn mine. Cassiterite is the other mineral most commonly found here. Wolframite has been found alongside cassiterite in granitic dikes which intrude limestone bedrock. Mining stopped in 1955 when crosscut trenches caved under rock pressure and flooded. Ten minerals are documented for this site, including wolframite, scheelite and pyrite.

Wolframite sample CR is from (Zinnwald) Cinvald Zapadocesky, Czech Republic. This is the same famous tin deposit previously mentioned: half in Bohemia

Czech Republic, half in Saxony Germany. Ninety minerals are documented for this site, including wolframite, hübnerite, ferberite, cassiterite, scheelite and tungstate.